Quarterly Report

Project Title:
Development of a Self-Sustained Wireless Integrated Structural Health Monitoring System for Highway Bridges

Cooperative Agreement # RITARS11HUMD

Eleventh Quarterly Progress Report

Period:
January 15, 2014 through April 14, 2014

Submitted by:
The Research Team – University of Maryland with North Carolina State University and URS

Submitted to:
Mr. Caesar Singh, Program Manager, US DOT

Date: April 28, 2014

Table of Contents

I — TECHNICAL STATUS

Accomplishments by Milestone

1.1. General

- Updated Project web site (http://www.ncrst.umd.edu/) (Task 1 and Deliverable 2)
- Delivered tenth quarterly financial and technical reports (Task 6 and Deliverable 11)
- Conducted group meeting with URS dated Jan. 22, 2014 on the summary of the past pilot bridge, I-270 over Middlebrook Road, and checked the status of the future demo bridge, I-95 over Patuxent River, and other possibilities.
- Attended TRB conference & NDE committee meeting in January 2014 in Washington, DC
- Plan to attend ASNT conference in August 2014 and delivered two abstracts.
- The revised work plan is shown below as Milestones/Deliverables. Dark Shading indicates Deliverable items and Tasks in which the Research Team has been engaged over the past quarters. Lighter shading indicates anticipated duration for Deliverables by quarters. Grid pattern shading means partially fulfilled.

Deliverables	Action	Quarter No.											
		1	2	3	4	5	6	7	8	9	10	11	12
1	Form TAC and conduct kick-off meeting. Determine baseline field test procedure (Task 1)												
2	Establish and update project web site (Tasks 1 & 6)												
3	Conduct baseline field test and finite element analysis on pre-selected bridges (Task 1)												
4	Design, fabricate and characterize AE sensor and measure the performance (Task 2)												
5	Develop and evaluate T-R method for passive damage interrogation (Task 3)												
6	Develop and experimentally evaluate wireless smart sensor and hybrid-mode energy harvester (Task 4)												
7	Implement passive damage interrogation T-R algorithm in the wireless smart sensor on bridges (Task 4)												
8	Integrate and validate AE sensors with wireless smart sensor and hybrid-mode energy harvester (Task 5)												
9	Develop and conduct field implementation/validation of commercial-ready ISHM system with remote sensing capability (Task 5)												
10	Recommend strategy to incorporate remote sensing and prognosis into BMS (Task 5)												
11	Prepare and submit quarterly status and progress reports and final project report (Task 6)												
12	Submit paper to conference presentations and publication to TRB meeting or other conferences (Task 6)												

Note: Deliverables items 7 for the 10th, 8, 9 and 10 for the 11th quarter are partially fulfilled. They are still tested and modified by the NCSU team. The explanation of the delay is described and highlighted later under Section 1.6 - Future Plan.

1.2. Remote Health Monitoring System

- Setup Data Acquisition and Sensing equipment on I95 Bridge with test site shown in Figure 1.

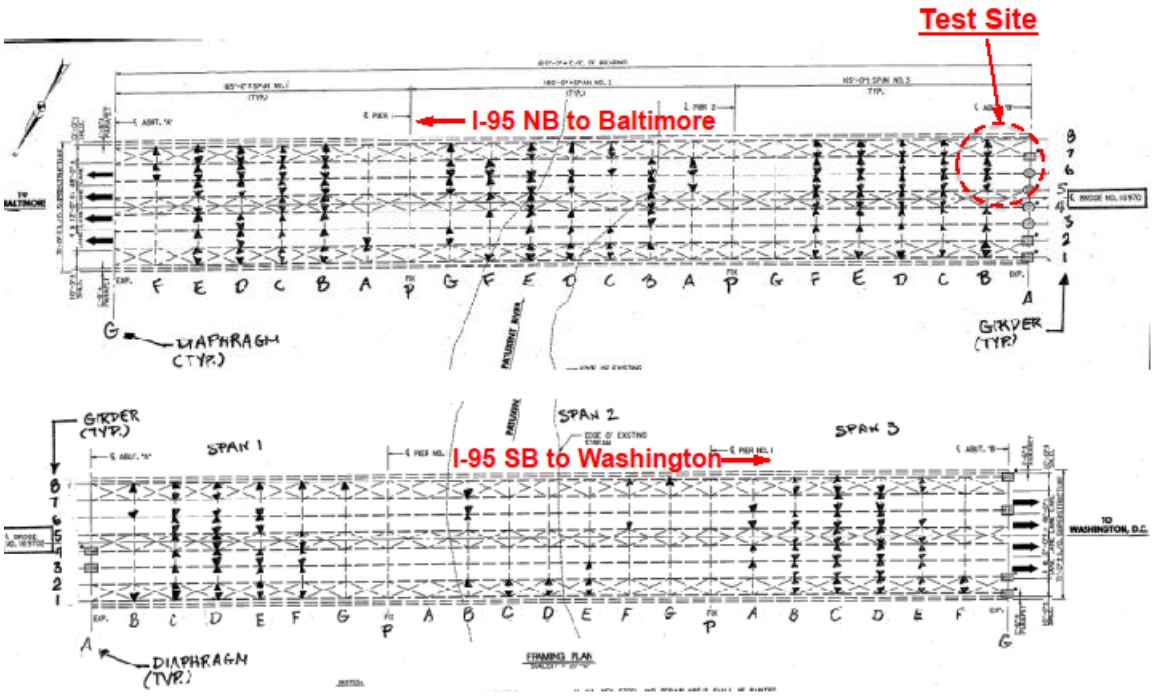

Figure 1 - – I95 bridge testing site and sensor locations

- Created Matlab program to read newly acquired Microstrain wireless sensor strain gauge and accelerometer data

- Created histograms of I270 acquired and extrapolated semi-annual S/N data

- Worked on I270 bridge dynamic performance under truck loading using ANSYS APDL
  - 3D finite element bridge model subjected to a moving vehicle
  - 3D finite element bridge model bridge subjected to a dynamic vehicle system (moving mass with spring and damper)
  - Vehicle-bridge interaction considering road roughness

- Worked on the influence on the stress of connection plates with or without top chords as well as skewed and non-skewed connection plate
  - The maximum axial force of top chords is small, around 2-3 kips, while the maximum axial forces of other chords are around 5 kips.
  - The stress of some elements of connection plates changes a lot. The conclusion can be reached after more elements have been checked.

1.3 Demo Bridge Test and following activities

- Acquired field measurements on I95 Bridge to acquire stress data and accelerometer data, which is complementary to the AE sensor data shown in Appendix A.

Description of the setup for the Microstrain wireless strain and accelerometer sensors and their collected data are shown in Appendix B.

- Used newly created Matlab program to read Microstrain wireless sensor strain gauge and accelerometer data

  - Ran the strain gauge data through rainflow counting program to find stress ranges
  - Ran accelerometer data into Fast Fourier Transform function to find the frequency of the bridge due to the traffic loading

- FEM analysis of Bridge No.1619701 I-95 NB over Patuxent River - The bridge No. 1619701 on I-95 over Patuxent River was built in 1965. It is a continuous three-span bridge with the middle span of 510 ft and two side spans of 165 ft. To investigate the fatigue performance of the bridge, a three-dimensional (3D) finite element model (Figure 2) is developed by using the CSiBridge™ for linear-elastic structural analyses. The model consists of eight I-girders. The depth of girder web is varied 6 ft at the abutment to 10 ft at the pier. The diaphragms are X-type bracing with top and bottom chord. The concrete deck, the girders were modeled by shell elements, while all the diaphragms and framing were modeled by truss element. The translations of x-, y-, z-directions are fixed at the abutments representing actual characteristics of support and continuity. The natural frequency of this model to match the field results is still under study.

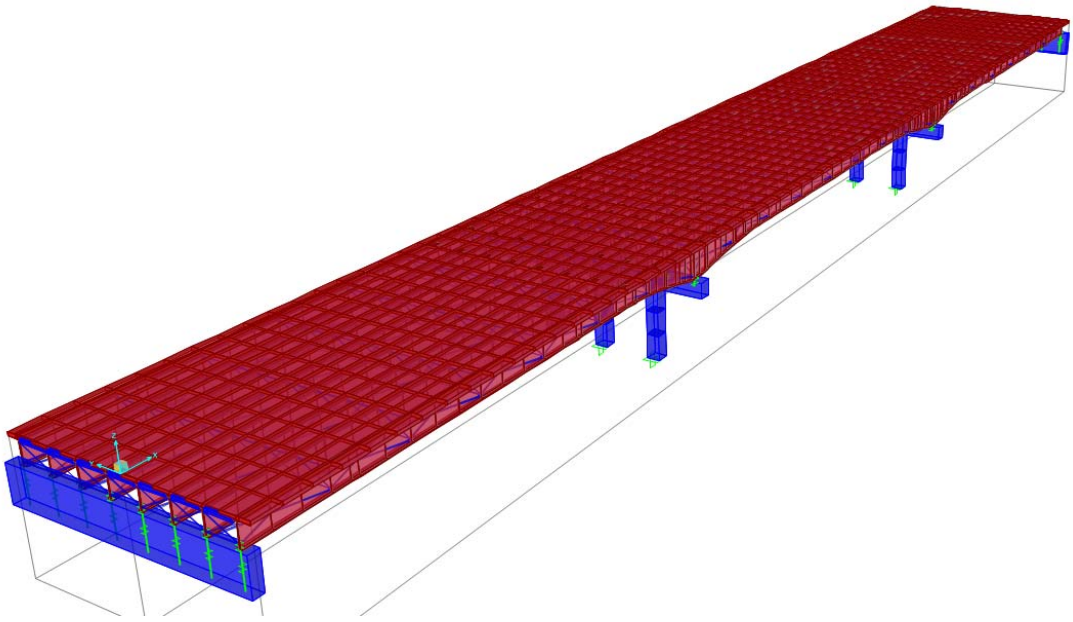

Figure 2 - – FEM model of I95 bridge

1.4 AE Sensor

Accomplishments by Milestone:

- A portable fatigue test setup has been designed and fabricated to test the piezo film AE sensor performance for fatigue crack induced AE signal monitoring. Figure 3(a) shows the portable test setup (laid on the ground) in the field test (conducted on March 14, 2014) at the I-95 Bridge. Figure 3(b) shows the test specimens after significant deformation was imposed on the test specimen, as evidenced by the tearing of the strain gage. Figure 4 shows the AE signals measured by piezo AE film sensor (Channel 0) and commercial AE sensor (SE1000-HI from Dunegan Engineering). Clearly, the piezo film AE sensor has a comparable level of sensitivity as the commercial wideband AE sensor. It is noted that commercial AE sensor measures out-of-plane displacement while piezo film AE sensor measures the in-plane strain and this explain why they have different waveforms.
- Field test of the piezo film acoustic emission sensors was carried out on the I-95 Bridge: Four piezo film AE sensors were surface mounted at locations near the existing fatigue cracks, as shown in Figure 5. The waveforms of AE signals acquired by these piezo film AE sensors and wireless sensor nodes show significant lower frequency contents but lacked higher frequency content (from 100 kHz to 300 kHz) typically associated with fatigue crack propagation. This observation confirmed the engineers' speculation with monitoring data, that is, the existing fatigue is inactive, and most likely the acquired AE signals were due to fracture surface rubbing and friction. Laser distance sensors were used to measure bridge girder deflection of Girder #2 and Girder #3 (girders where fatigue cracks were monitored). The locations of the girders where deflections were measured were approximately 48'-10" from the south bridge abutment. Peak displacement of 5 mm and 6 mm were recorded for Girder #2 and Girder #3 respectively during a 1-hour recording for each of these two girders.

(a) (b)

Figure 3 - Acoustic emission sensor test using portable fatigue test setup: (a) field test at I-95 Bridge in Maryland; (b) close up view of piezo film AE sensors on test specimen

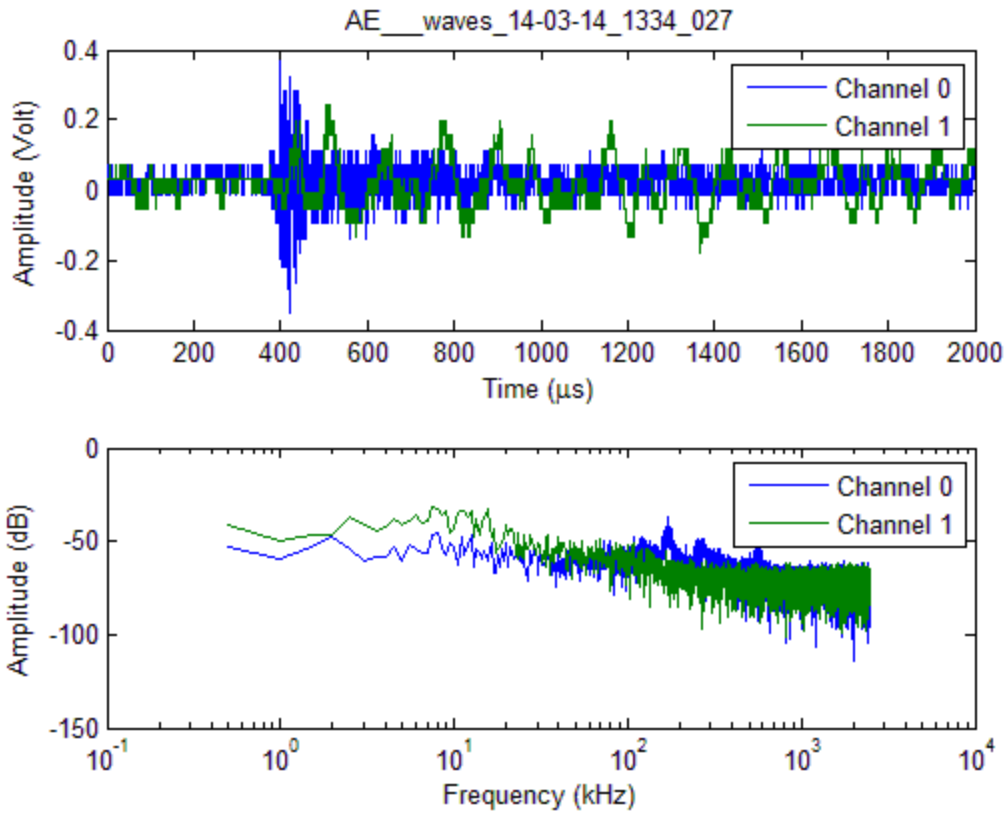

Figure 4 - Acoustic emission signal recorded by the piezo film AE sensor (channel 0) and commercial wideband AE sensor (HI-1000 by Dunegan Engineering) when the notched steel plate test specimen underwent significant deformation

Figure 5 - Piezo film AE sensors installed on Girder #2 of I-95 Bridge to monitor existing fatigue crack

Figure 6 - Laser distance sensor to measure deflection of Girder #2 of I-95 Bridge

1.5 T-R Method, Energy Harvesting and Smart Sensor

Accomplishments of these tasks by UMD/NCSU team are summarized here:

Accomplishments by milestone:

1. Finished soldering and preparing all wireless piezoelectric sensors.

Figure 7 - Soldered Wireless Piezoelectric Sensor PCB

Figure 8 - Wireless Piezoelectric Sensor

2. Conducted field test on the I-95 NB Bridge over Patuxent River in Maryland.

   Date: March 10 to March 15, 2014
   Bridge Site: latitude= 39.114742, longitude= -76.873653, I-95 NB Bridge over Patuxent River.
   Participants:
   Dr. C. C. Fu (UMD), Dr. Y. Zhang (UMD), Dr. Zhou (URS)
   Tim Saad (UMD), Fan Zhang (UMD), Ruipeng Li (UMD), Chao Wan (NCSU)

Figure 9 - I-95 NB Bridge over Patuxent River

Figure 10 - Test Platform under the Bridge

Figure 11 - Wireless AE Sensor (Left) and Crack (Right)


Figure 12 - Wireless AE Sensor (Left) and Crack (Right)

3.

Figure 13 - Solar Panel (Left) and Wind Turbine (Right)

Test Results on the I-95 NB Bridge:

Conducted traffic tests by using wireless AE sensors on March 12th and March 14th. We got seven times triggered signal on March 12th and twelve times on March 14th. Those results are covered in Appendix A.

1.6 Future Plans

Demo Bridge Testing (UMD team led by Dr. Fu) –

- Working with MDSHA on the demo bridge (I-95 over Patuxent River).
- Preparing for the May 2014 test and coordinating with all field team members.
- Collecting W-I-M data on I-95 Bridge to simulate traffic through FEM models for all pilot test bridge in Maryland and validating test data with FEM results.
- Refining the local finite element model of the crack location, doing the same analysis with the global model, comparing the results and discussing the necessarily of local model for our studies.
- Determining which of the four possible crack configurations has the highest SIF at the crack tip and thus most likely to occur using finite element model.
- Estimating fatigue failure using Wohler Curve (S-N curve) through the collected strain data where their results are currently undergoing analysis and comparisons with a probabilistic model for fatigue damage.
- Reviewing I270 bridge model dynamic performance for practical consideration and considering applying to the I95 bridge
  - Beam model under truck flow
  - Grid model under truck flow

AE Sensor (UMD team led by Dr. Zhang) -

- Field test in May and June 2014 is planned to further test the integrated wireless sensor system through on-site fatigue crack growth monitoring. Remote sensing features will be examined and improved based on field test results on the steel highway bridge on the Patuxent River along I-95 in Maryland.
- Data processing and feature analysis of AE signal data recorded from a portable fatigue test setup to be mounted on I-95 Bridge will be conducted.

T-R Method, Energy Harvesting and Smart Sensor (NCSU team led by Dr. Yuan) -

- Optimize the program of the wireless piezoelectric sensor.
- Optimize the GUI program of the wireless piezoelectric sensor system.
- Prepare for the filed test on the I-95 NB Bridge over Patuxent River in May.

II — BUSINESS STATUS

- Hours/Effort Expended – As the last reporting period, PI Dr. Fu worked one month paid by his cost sharing account for 167 man-hours. Three (3) UM and two (2) NCSU graduate assistants worked three months half-time (20 hours), the quarterly accounting deadline, for a total of 1,470 man-hours (one NCSU assistant is partially cost-shared by their University.)
- Total Budget - $1,151,169 & Invoiced (3/31/14) - $985,401.49 (85.6%)
- Cost sharing committed - $1,525,063 & Cost shared (3/31/14) - $1,179,279.64 (77.3%, which is now over the federal share total of $1,151,169).

Appendix A

Field Test AE Results
of
Bridge No.1619701 I-95 NB over Patuxent River

2014-03-12 Test 1

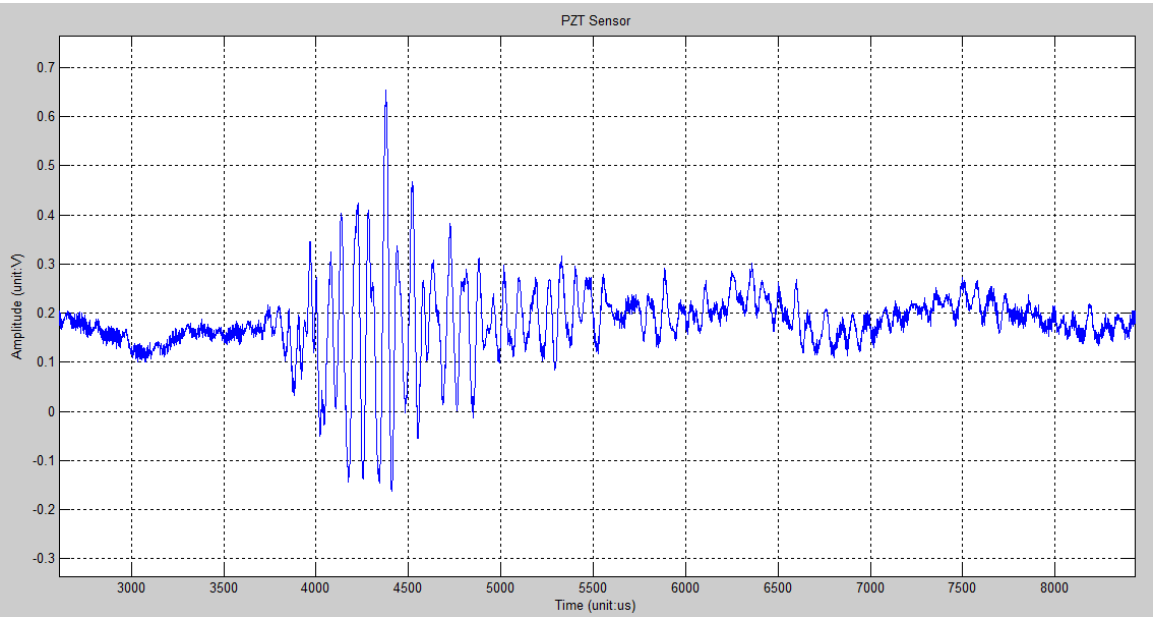

The signal from PZT sensor

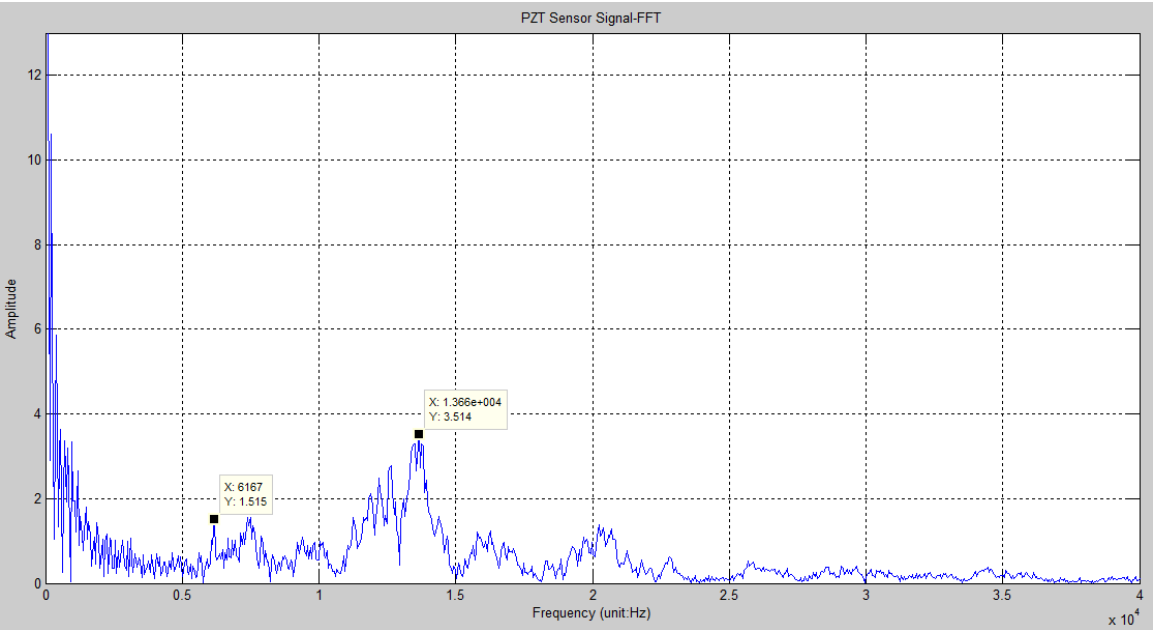

Figure A.1 - The FFT result of the PZT sensor's signal

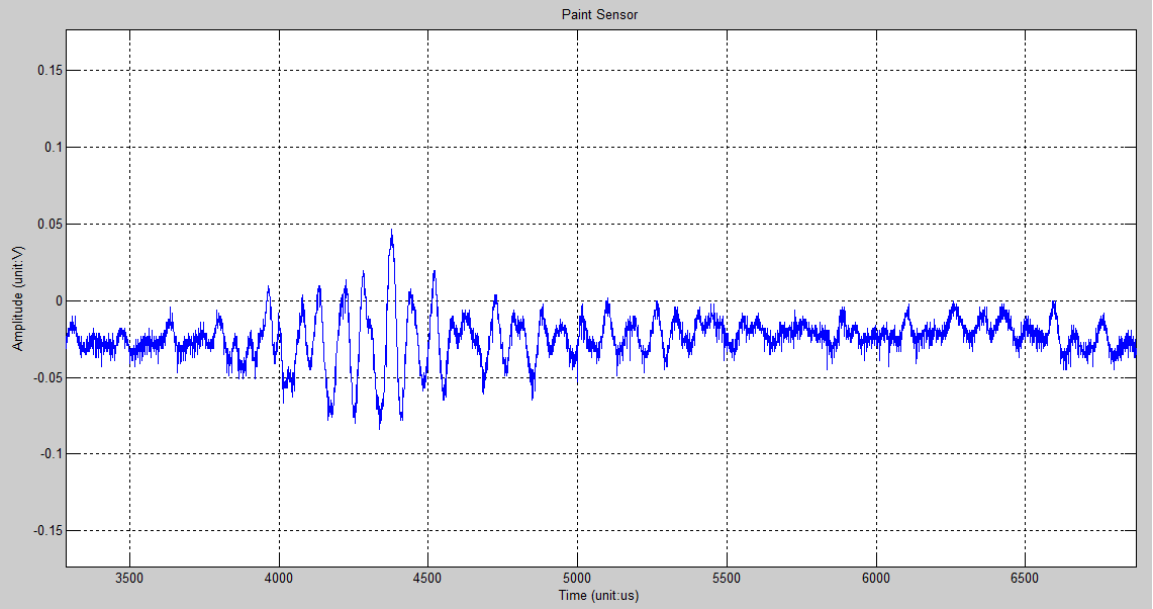

The signal from Paint sensor

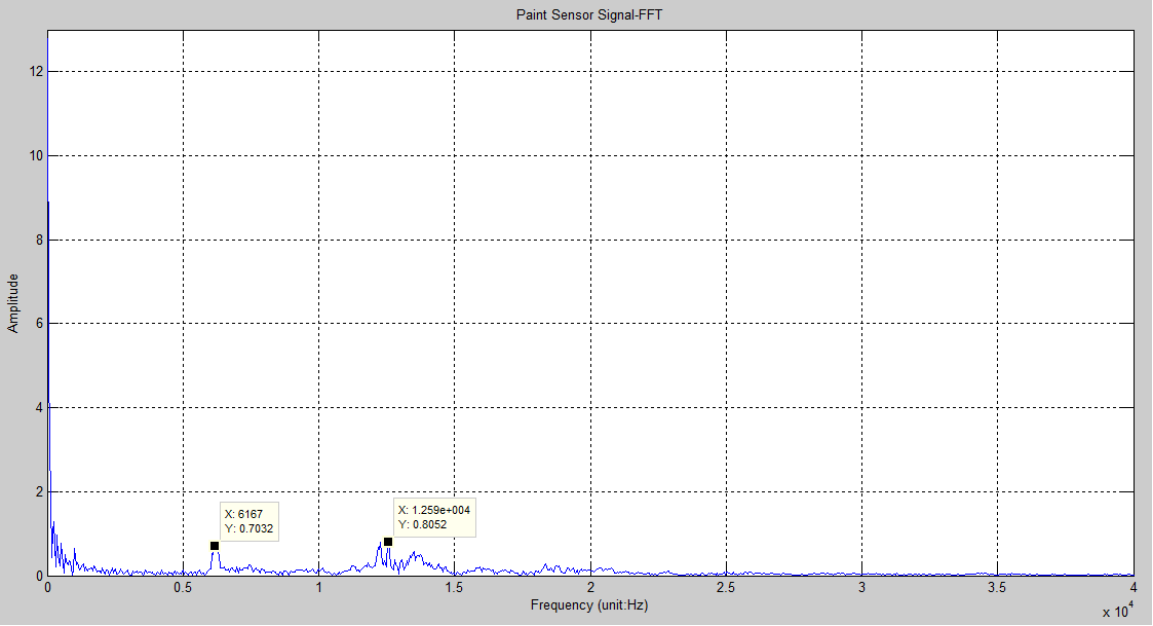

Figure A.2 - The FFT result of the Paint sensor's signal

20140312Test2

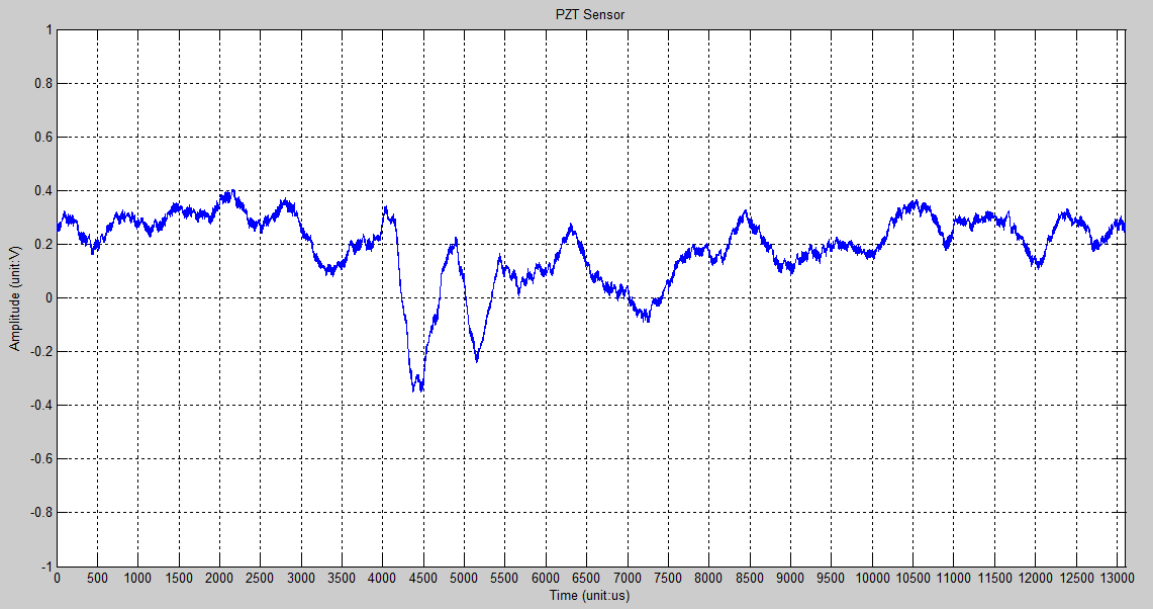

The signal from PZT sensor

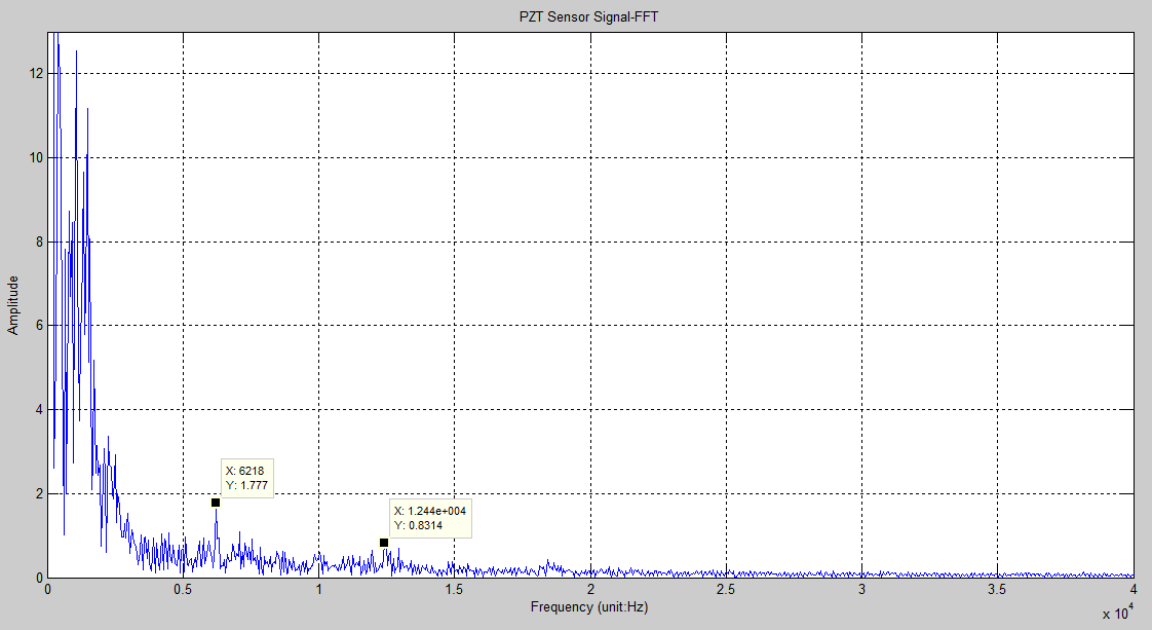

Figure A.3 - The FFT result of the PZT sensor's signal

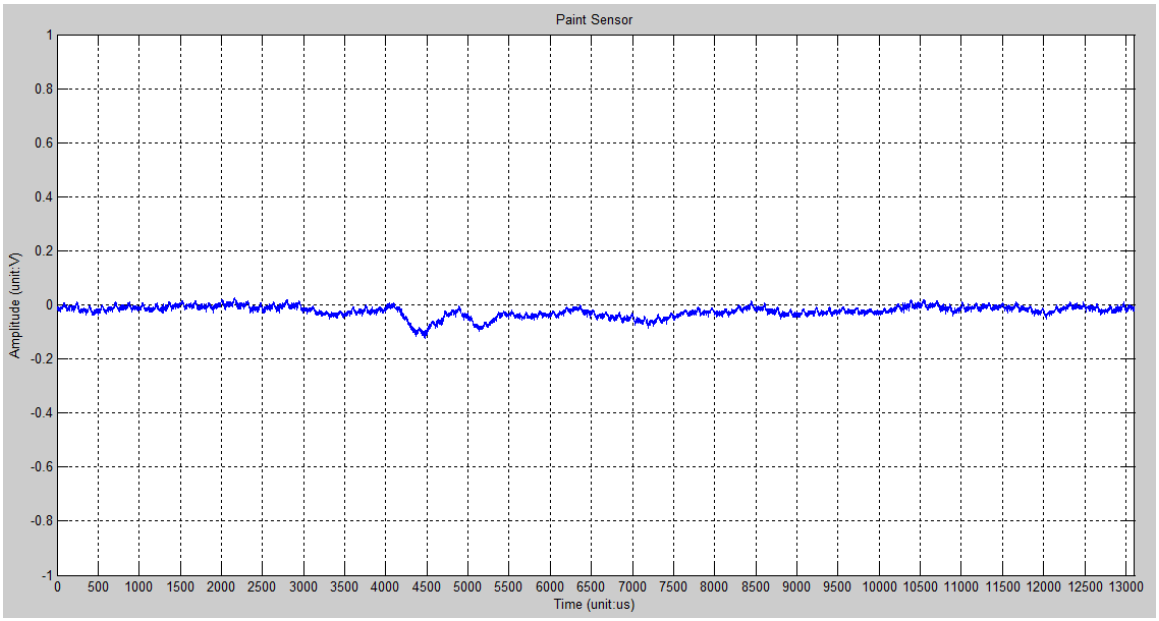

The signal from Paint sensor

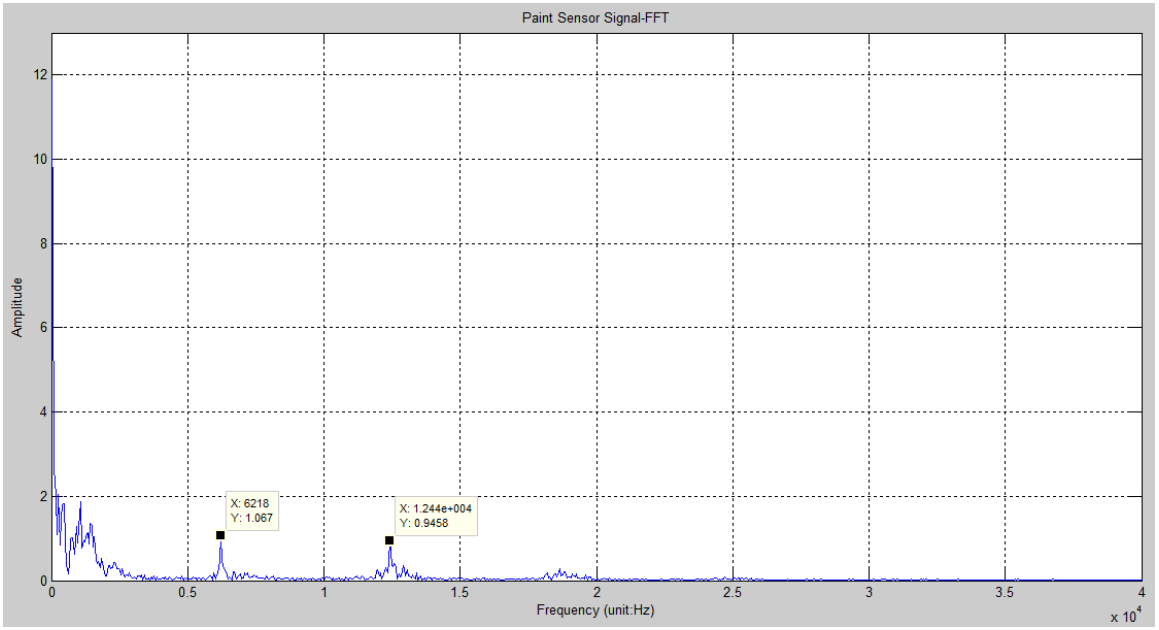

Figure A.4 - The FFT result of the Paint sensor's signal

2014-03-12 Test 3

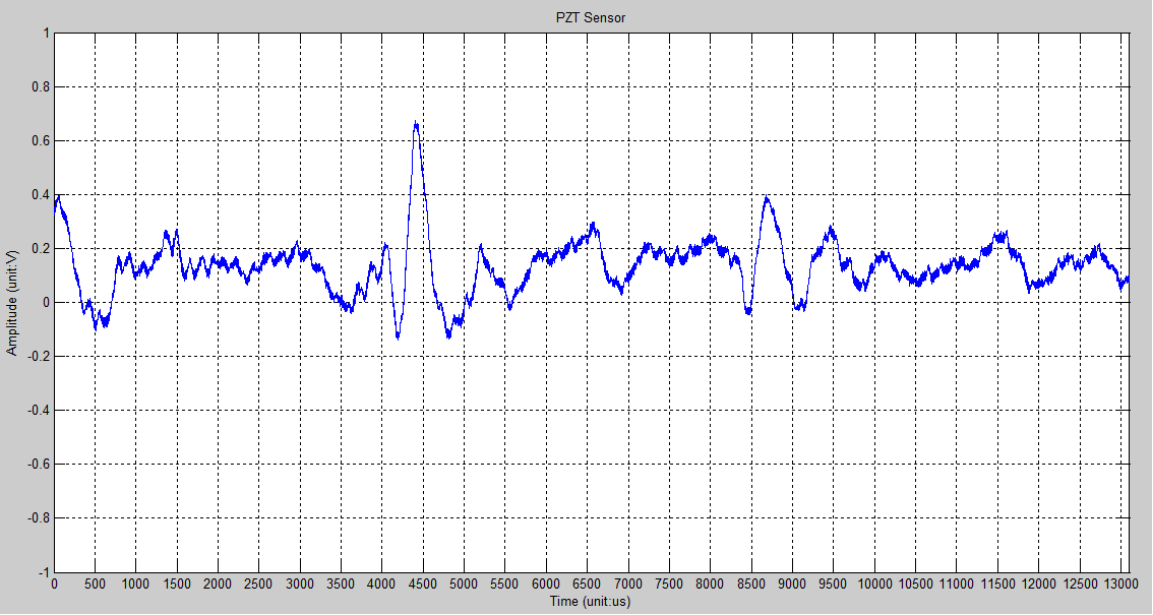

The signal from PZT sensor

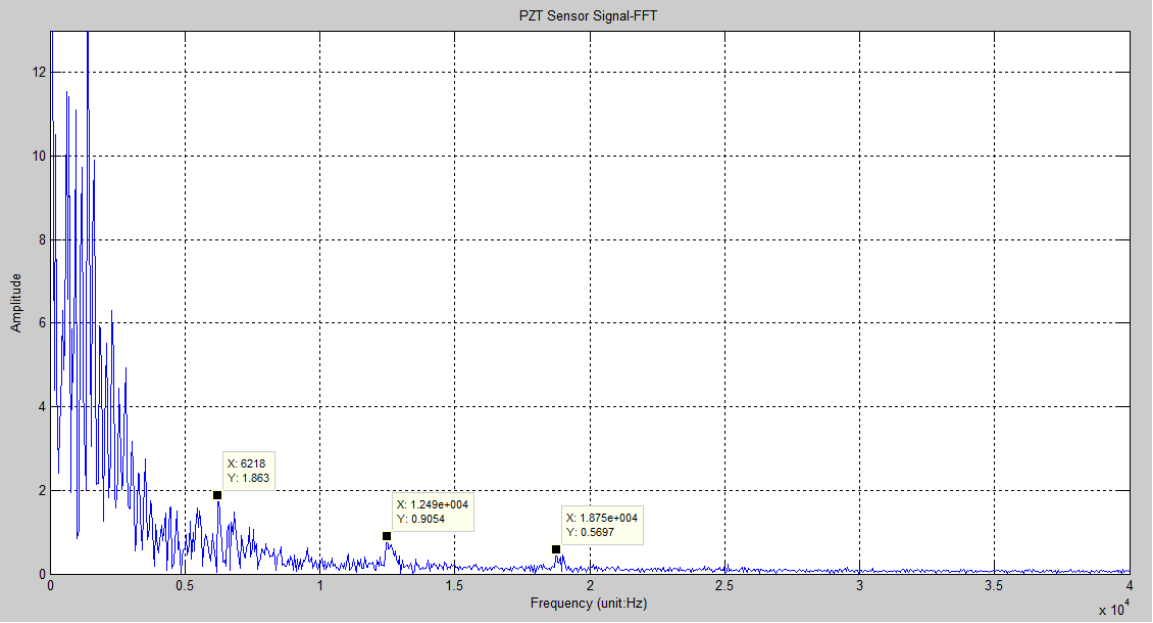

Figure A.5 - The FFT result of the PZT sensor's signal

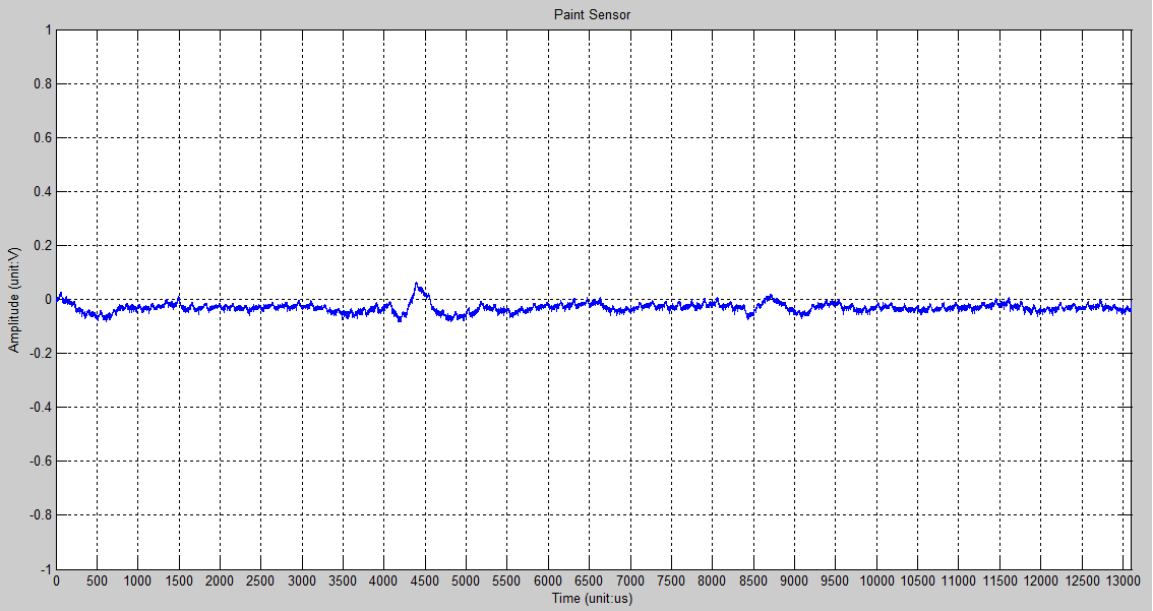

The signal from Paint sensor

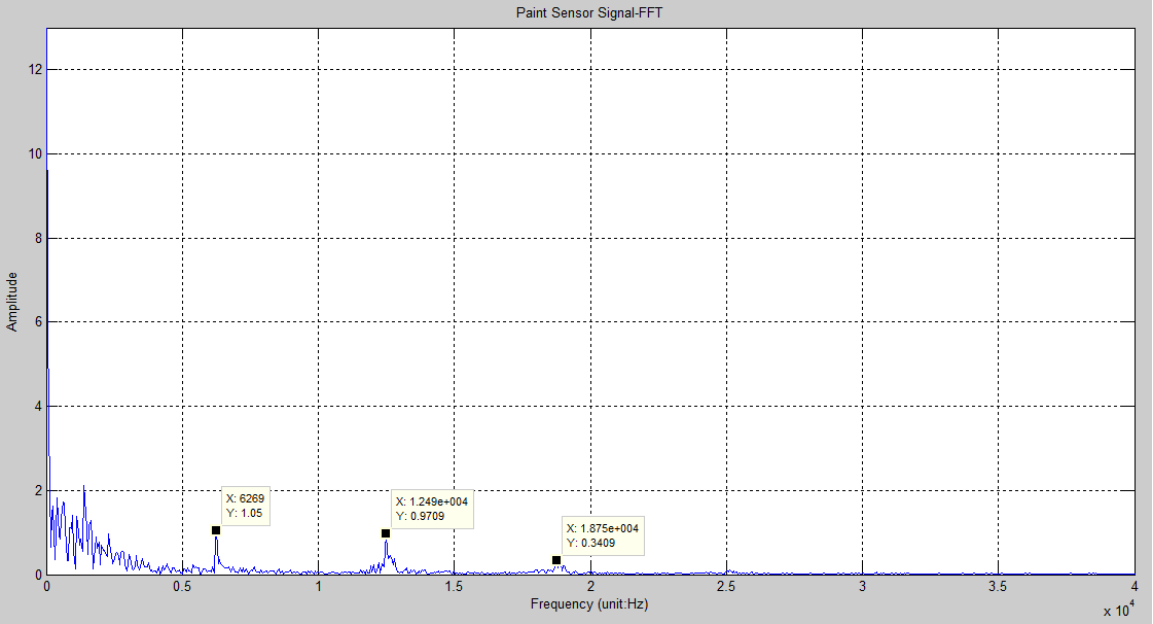

Figure A.6 - The FFT result of the Paint sensor's signal

2014-03-12 Test 4

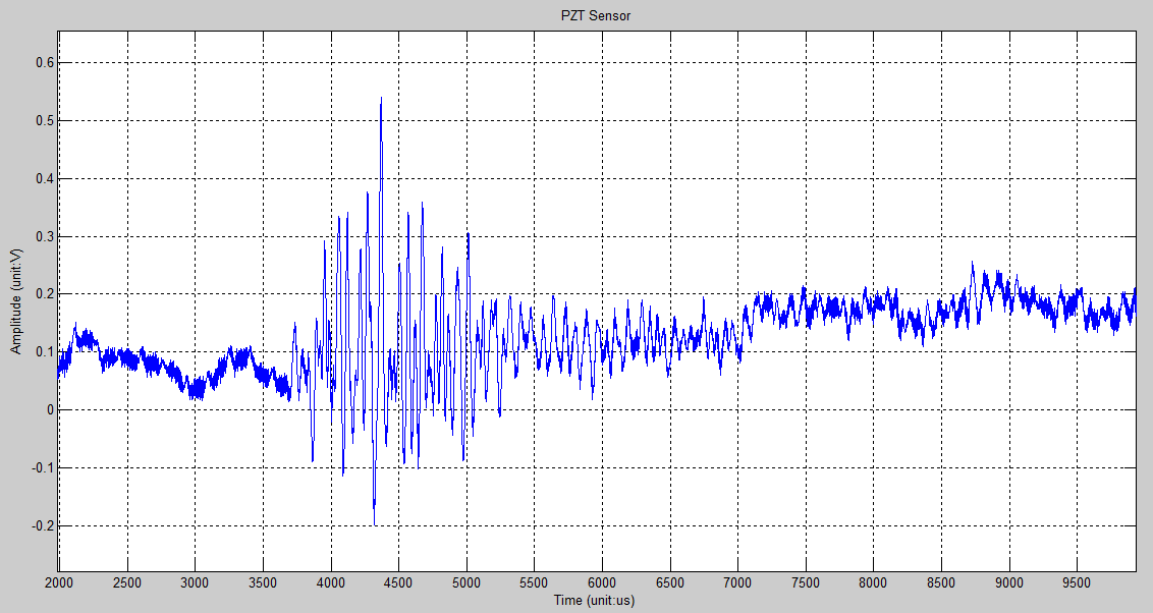

The signal from PZT sensor

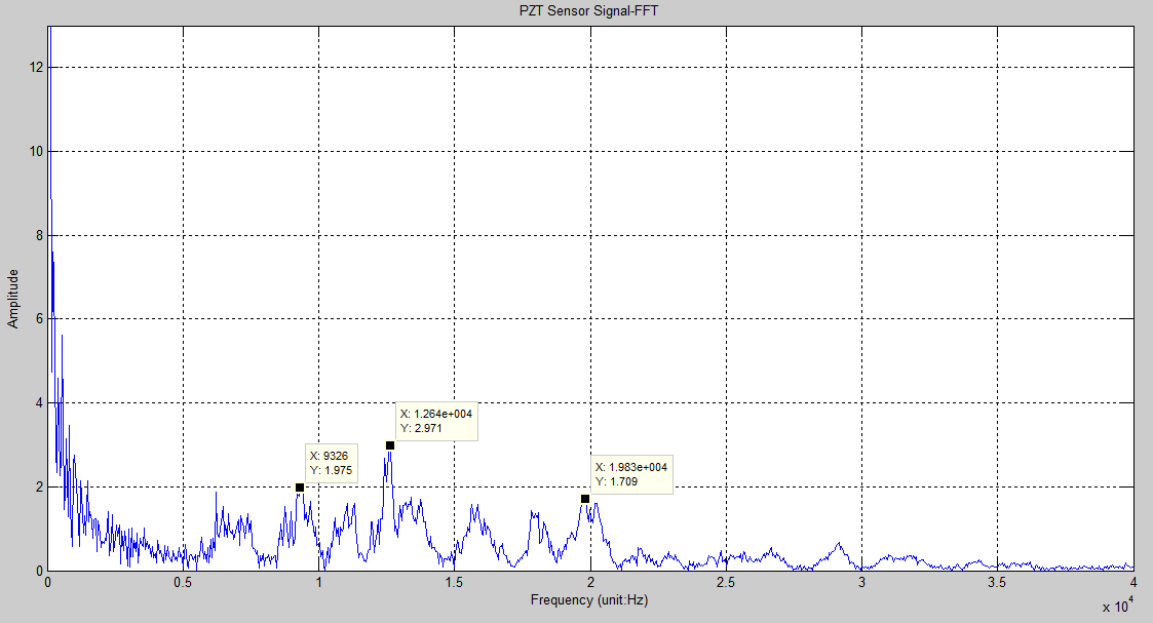

Figure A.7 - The FFT result of the PZT sensor's signal

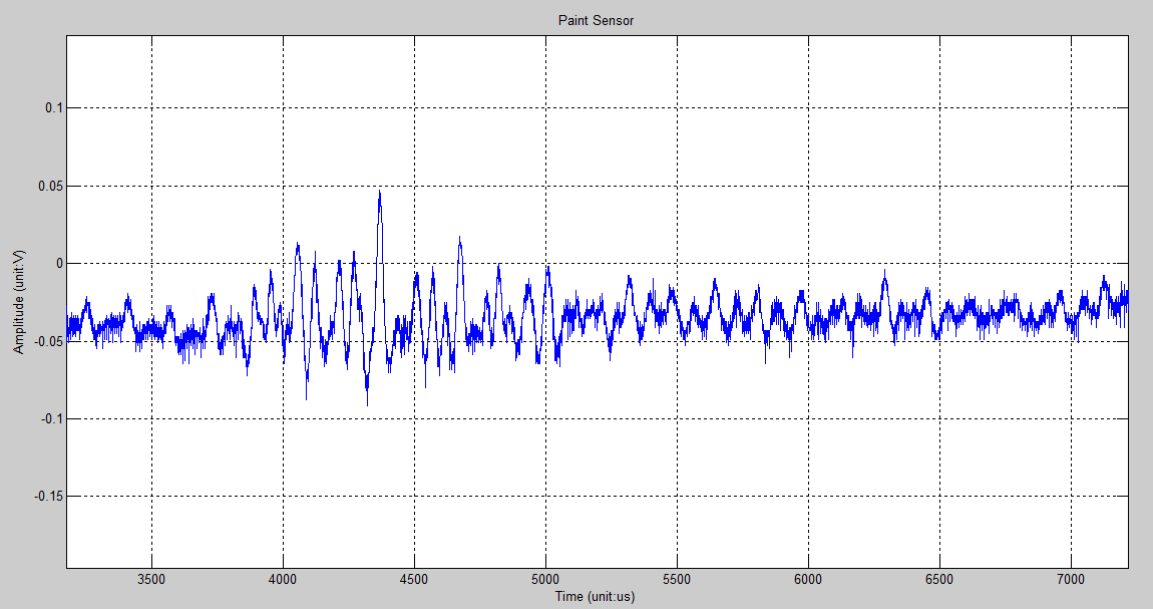

The signal from Paint sensor

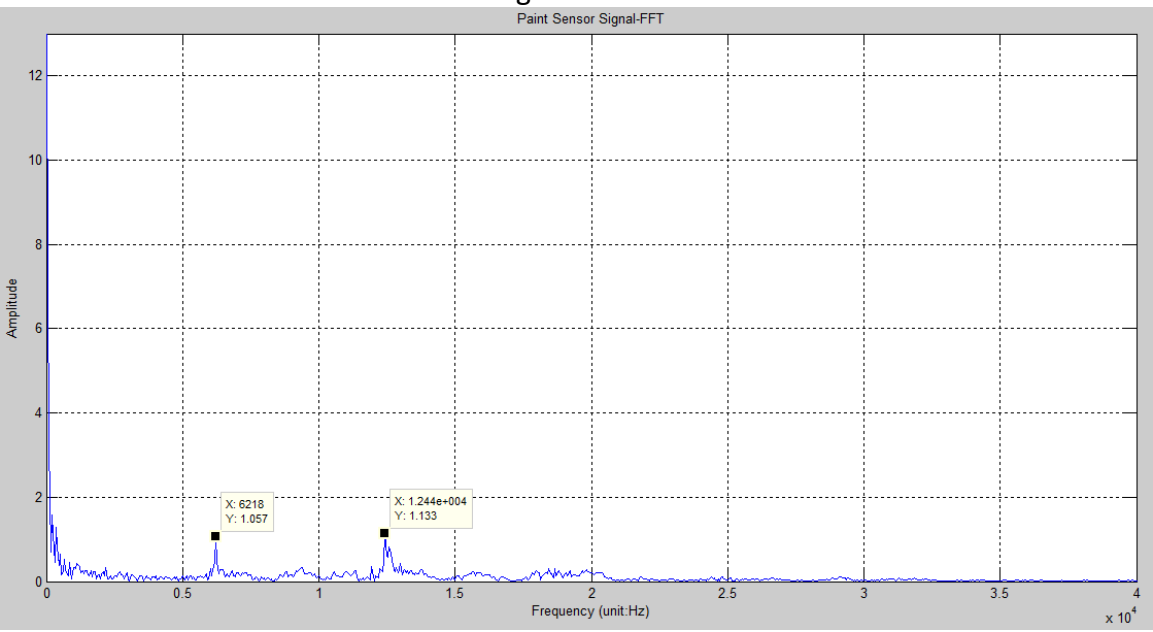

Figure A.8 - The FFT result of the Paint sensor's signal

2014-03-12 Test 5

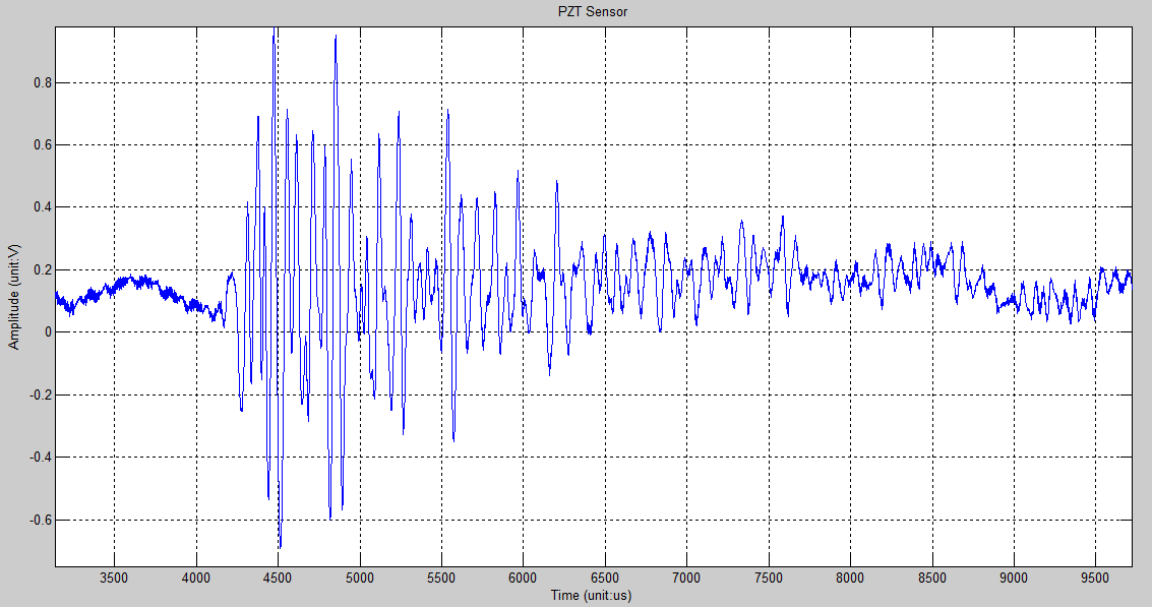

The signal from PZT sensor

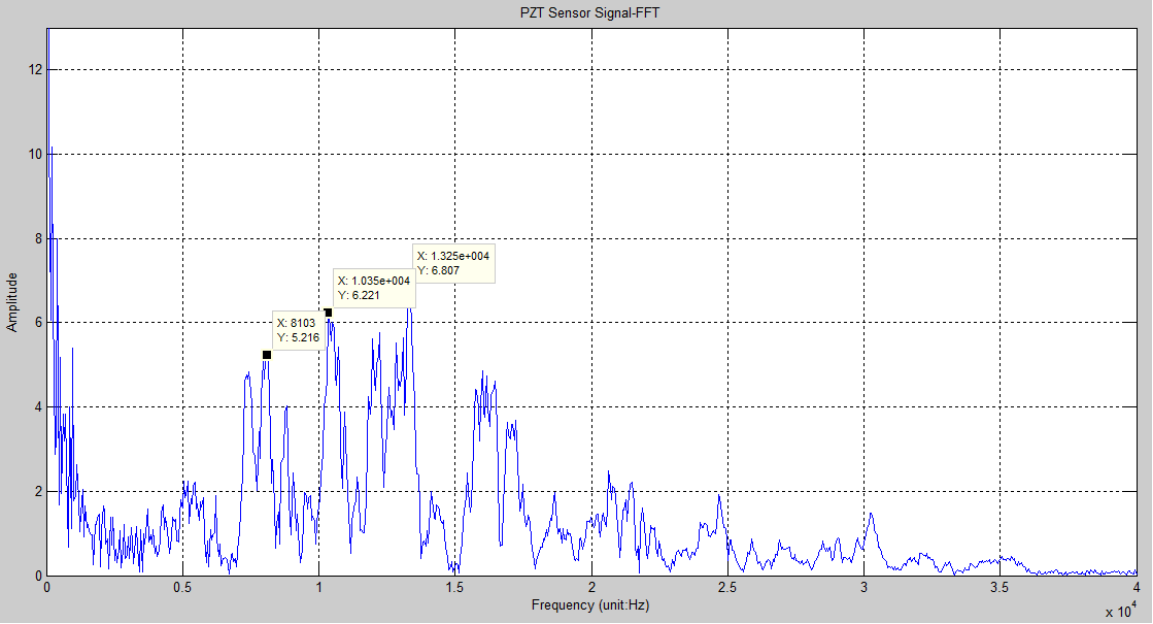

Figure A.9 - The FFT result of the PZT sensor's signal

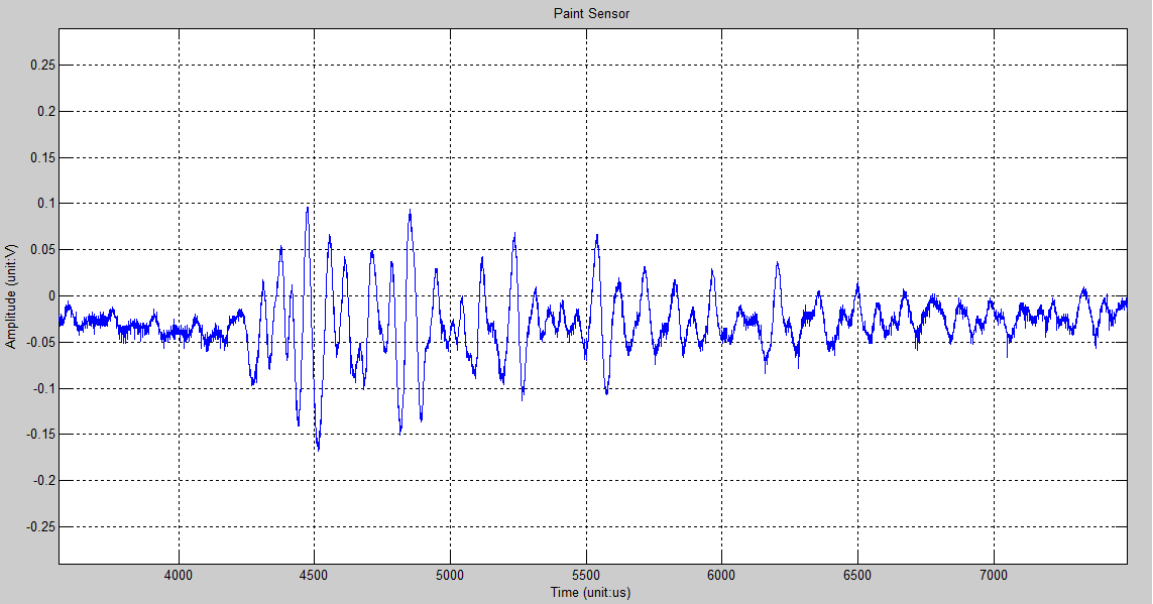

The signal from Paint sensor

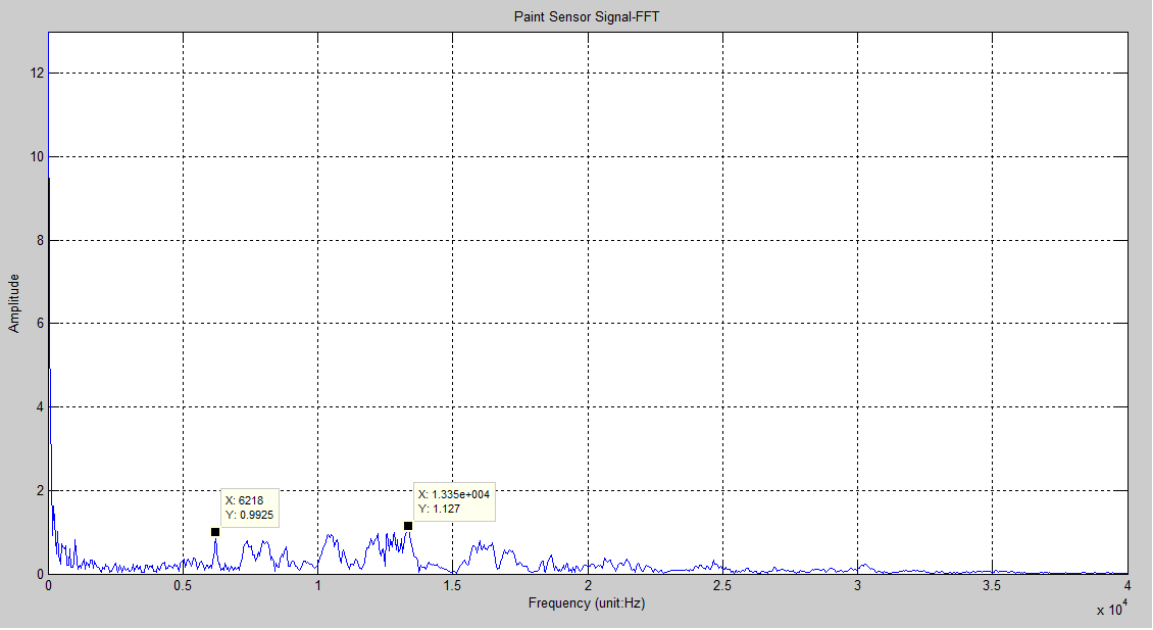

Figure A.10 - The FFT result of the Paint sensor's signal

2014-03-12 Test 6

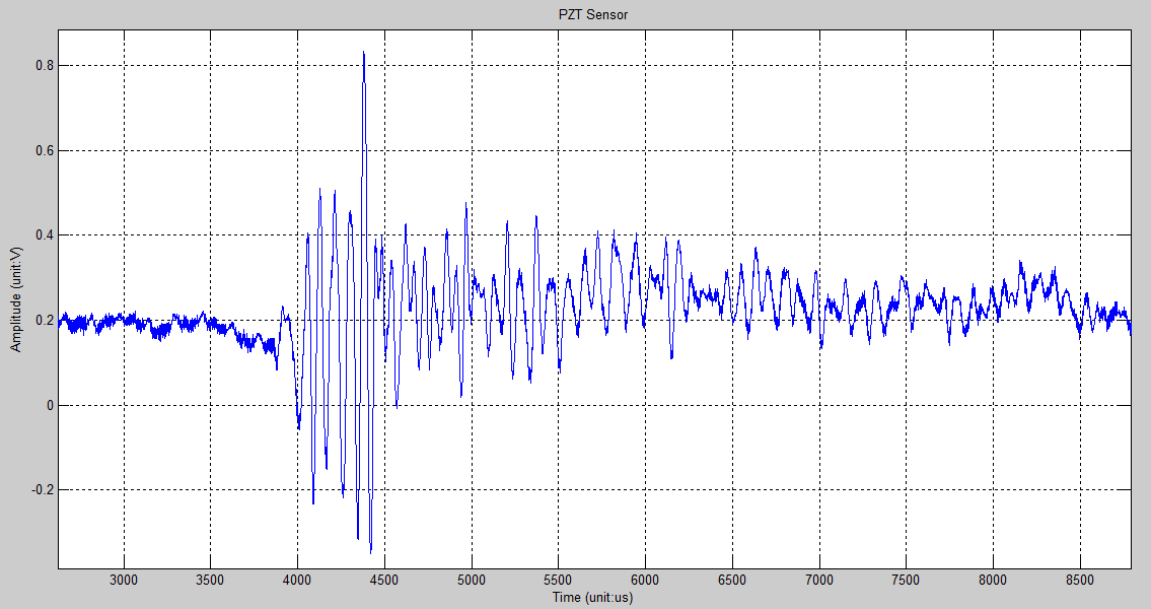

The signal from PZT sensor

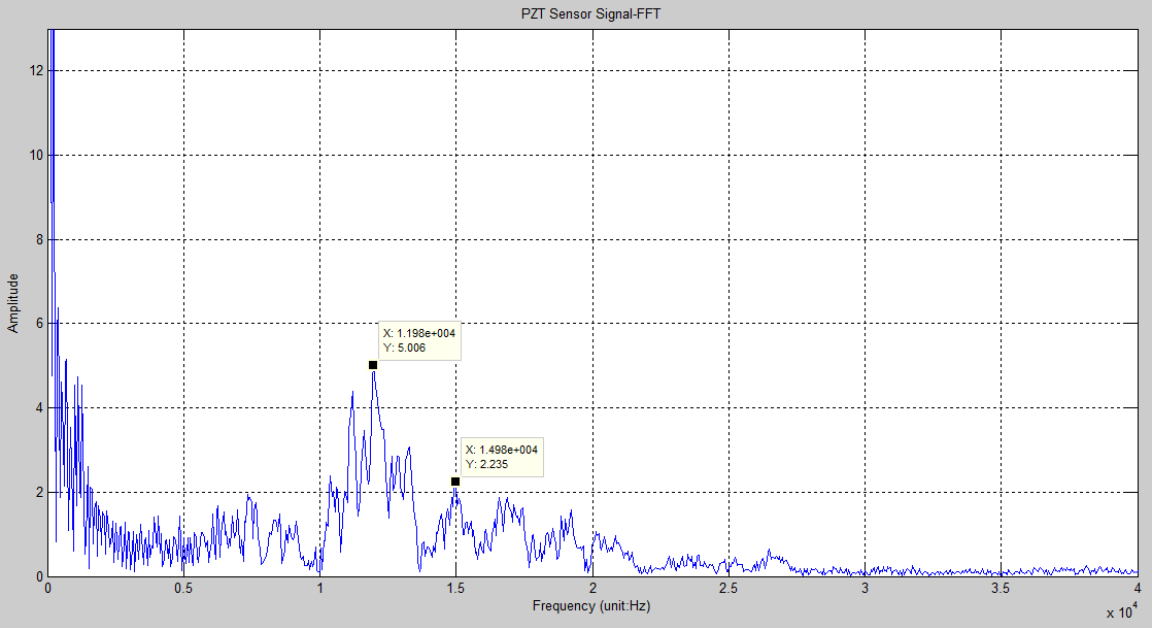

Figure A.11 - The FFT result of the PZT sensor's signal

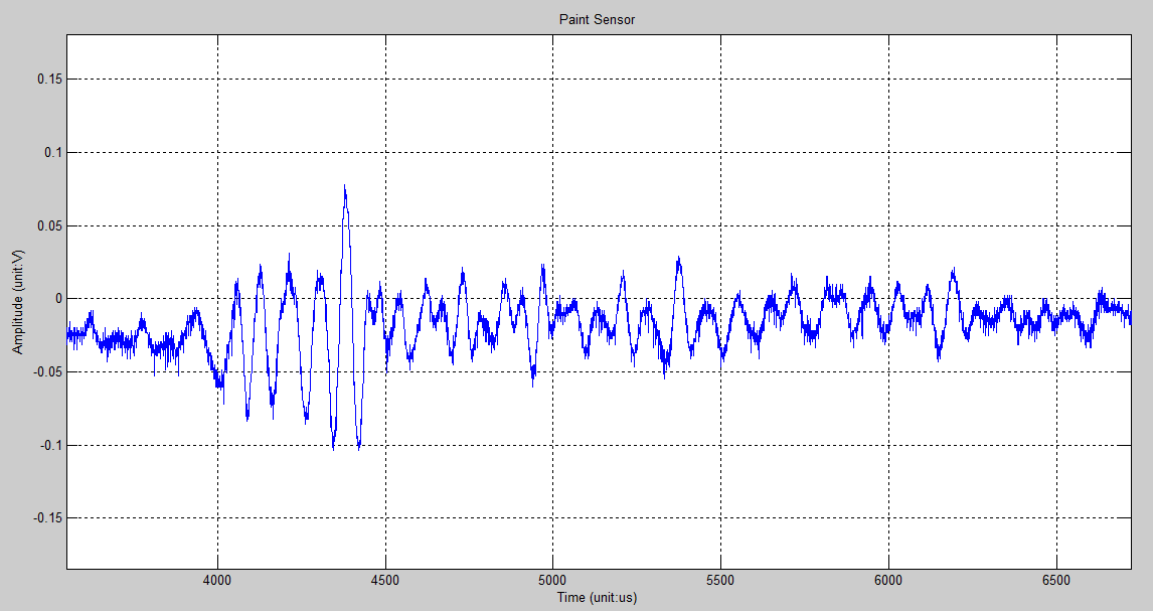

The signal from Paint sensor

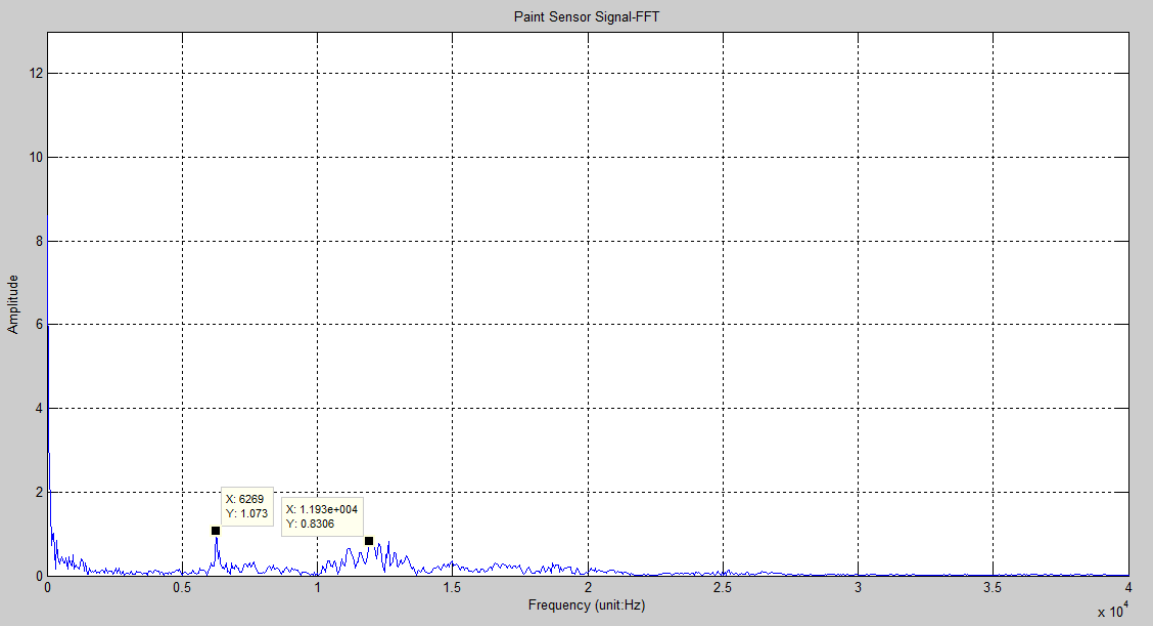

Figure A.12 - The FFT result of the Paint sensor's signal

2014-03-12 Test 7

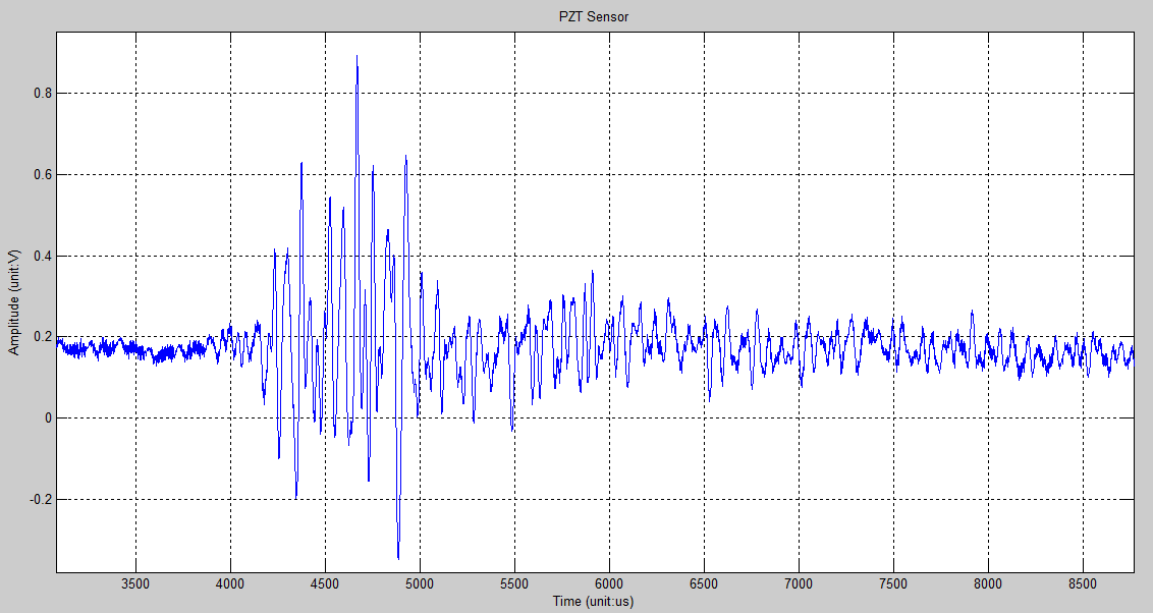

The signal from PZT sensor

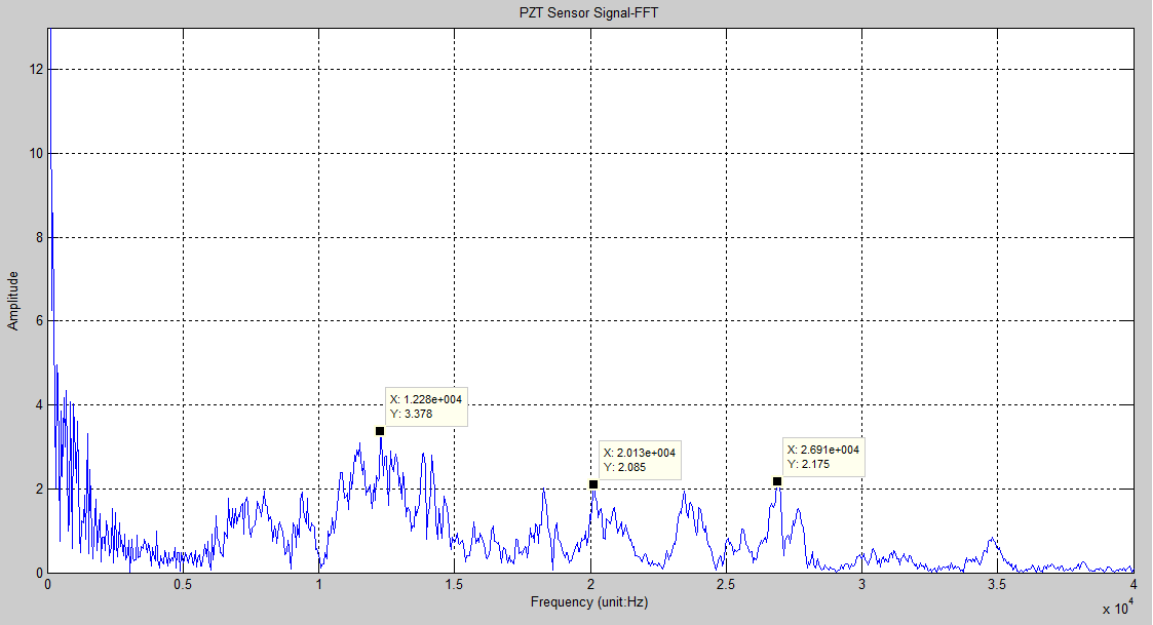

Figure A.13 - The FFT result of the PZT sensor's signal

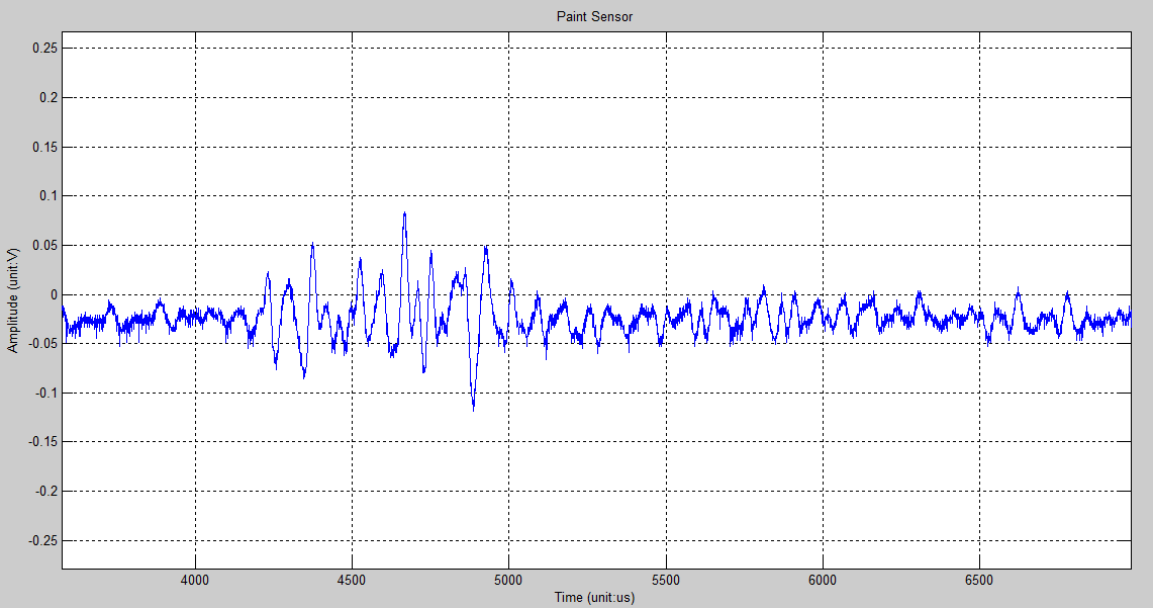

The signal from Paint sensor

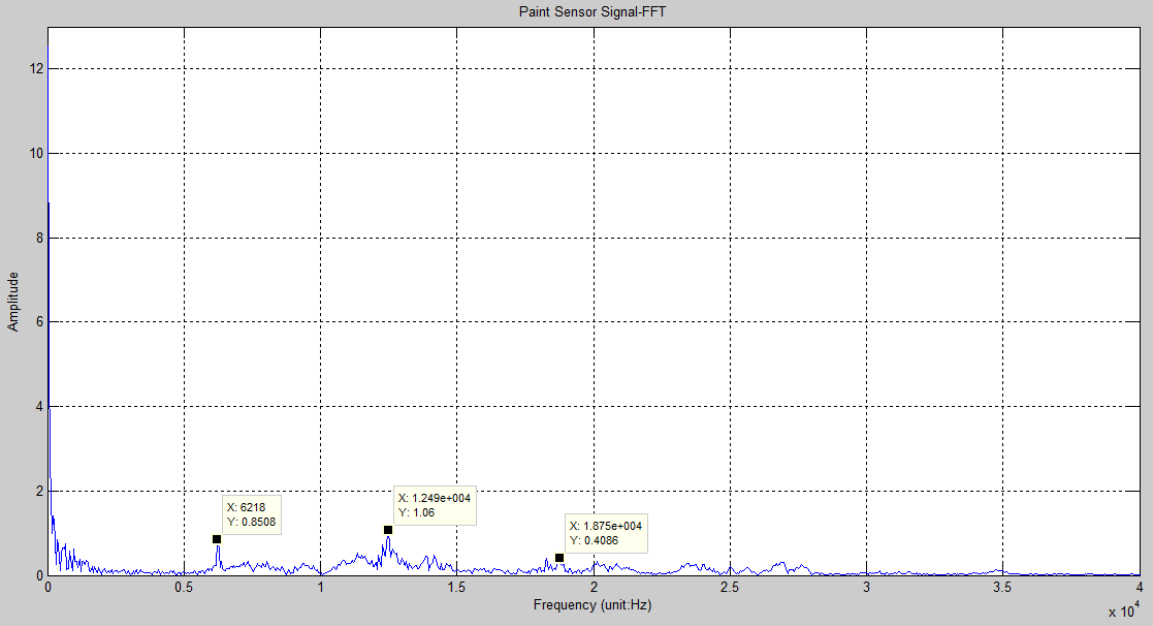

Figure A.14 - The FFT result of the Paint sensor's signal

2014-03-14 Test1 (Time: 13:17:50)

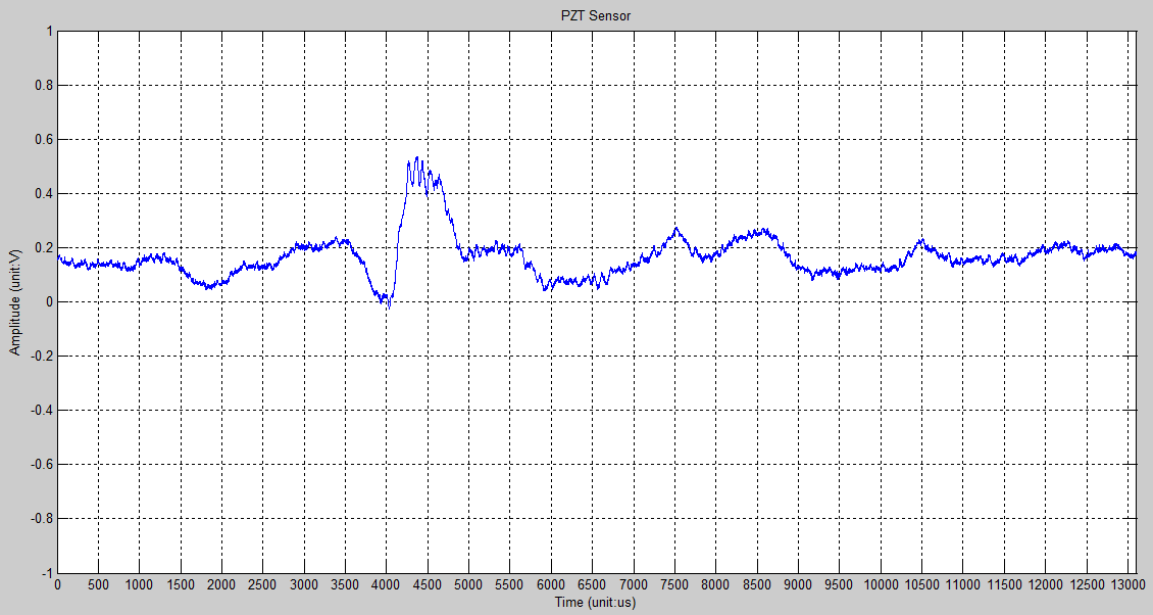

The signal from PZT sensor

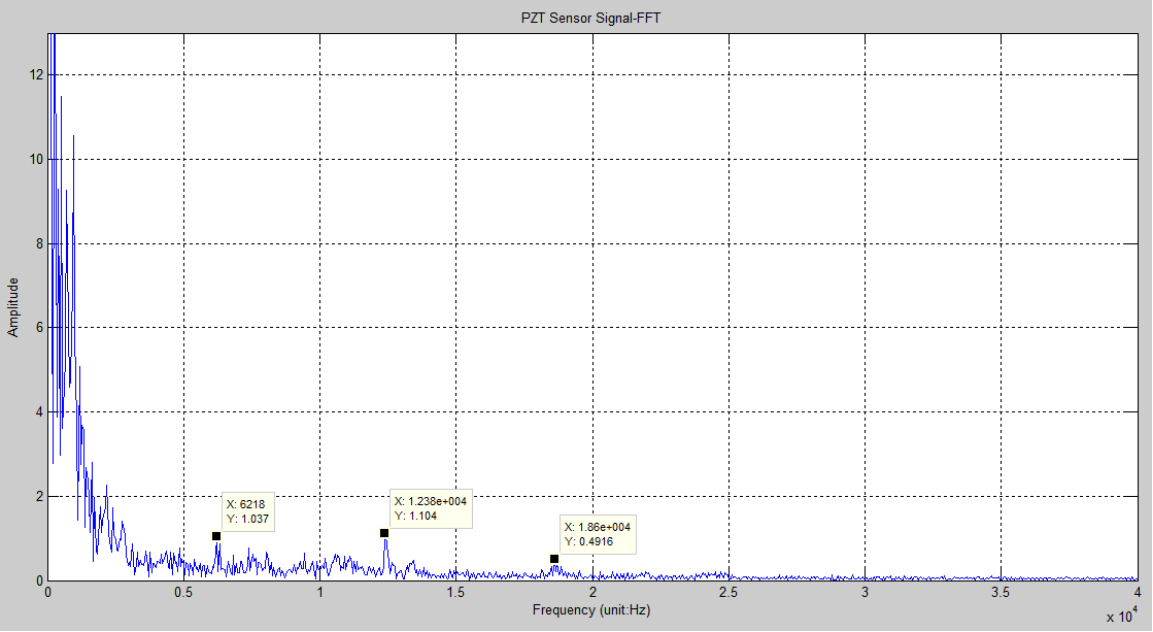

Figure A.15 - The FFT result of the PZT sensor's signal

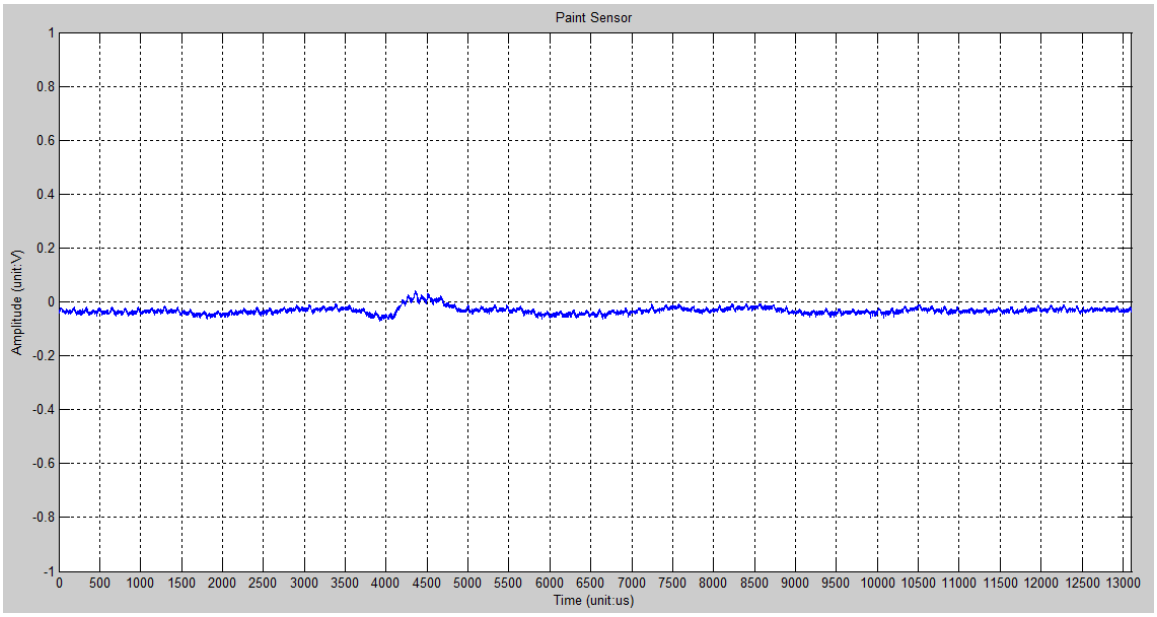

The signal from Paint sensor

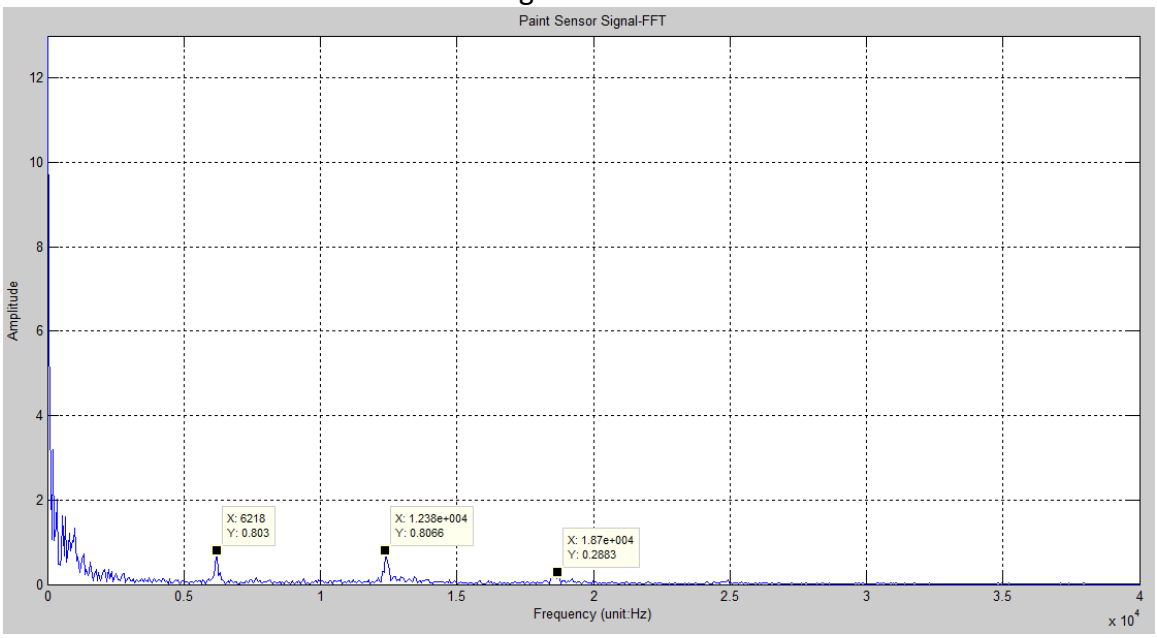

Figure A.16 - The FFT result of the Paint sensor's signal

2014-03-14 Test2 (Time: 13:22:39)

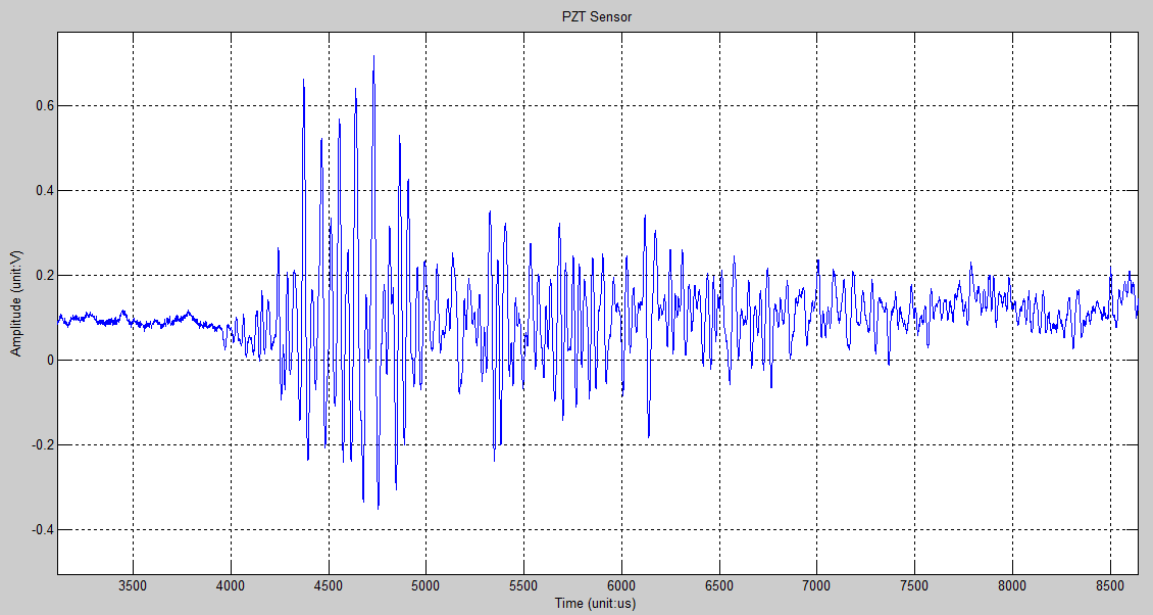

The signal from PZT sensor

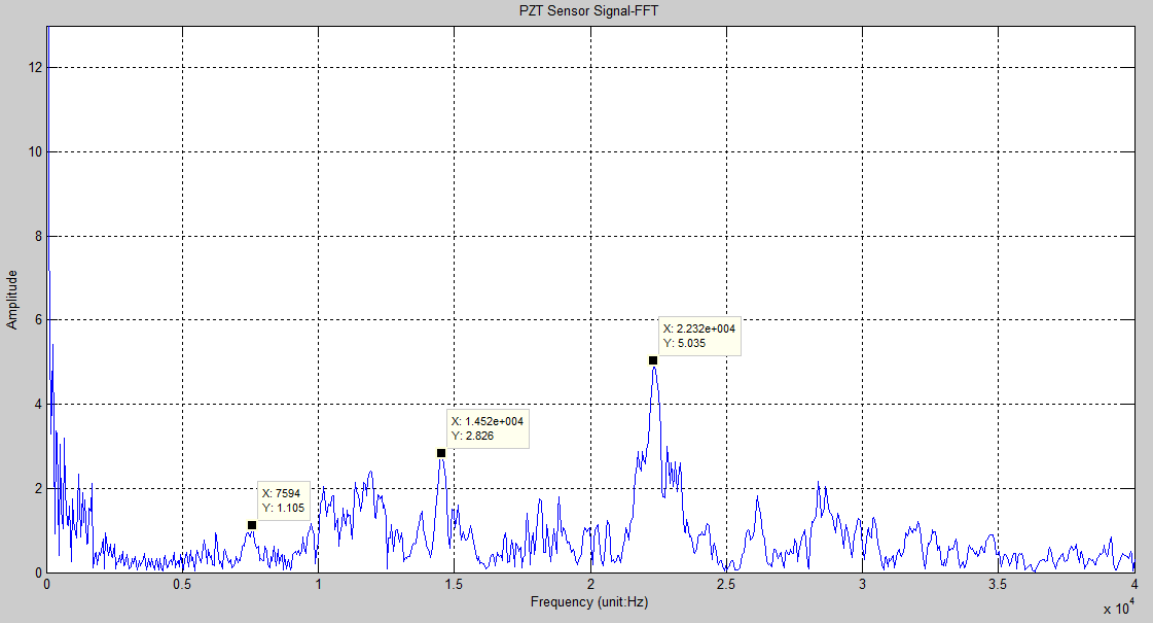

Figure A.17 - The FFT result of the PZT sensor's signal

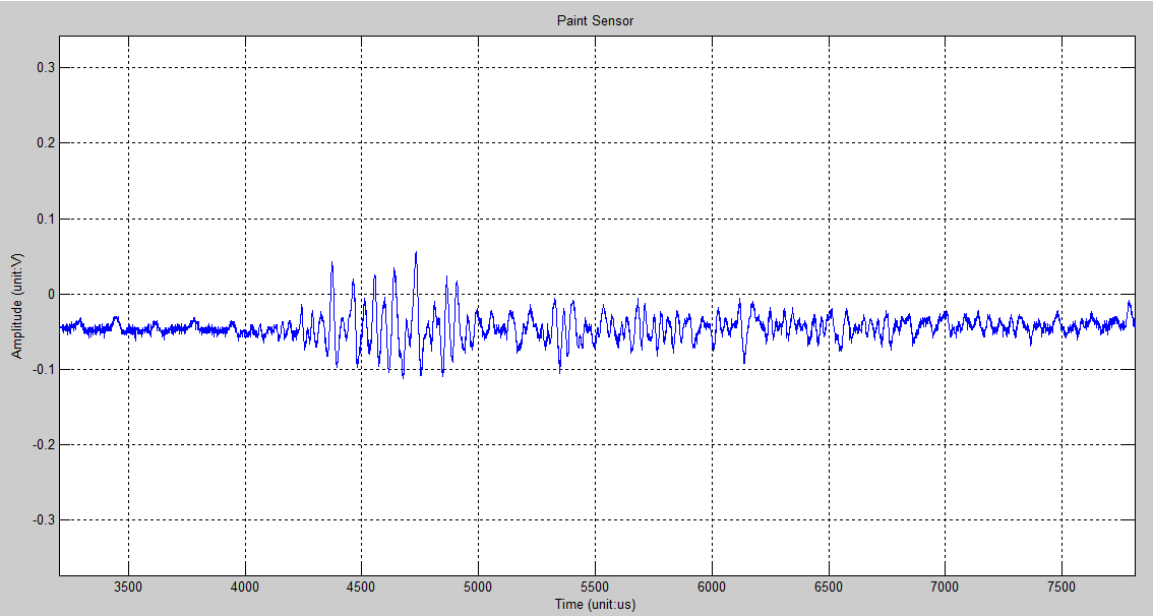

The signal from Paint sensor

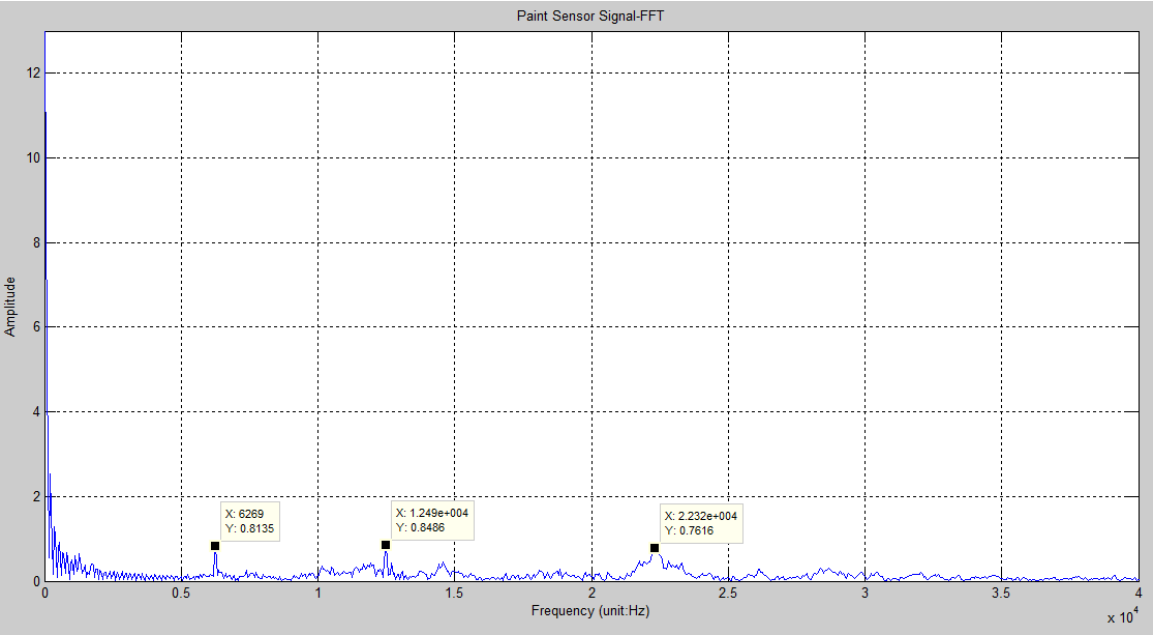

Figure A.18 - The FFT result of the Paint sensor's signal

2014-03-14 Test3 (Time: 13:26:31)

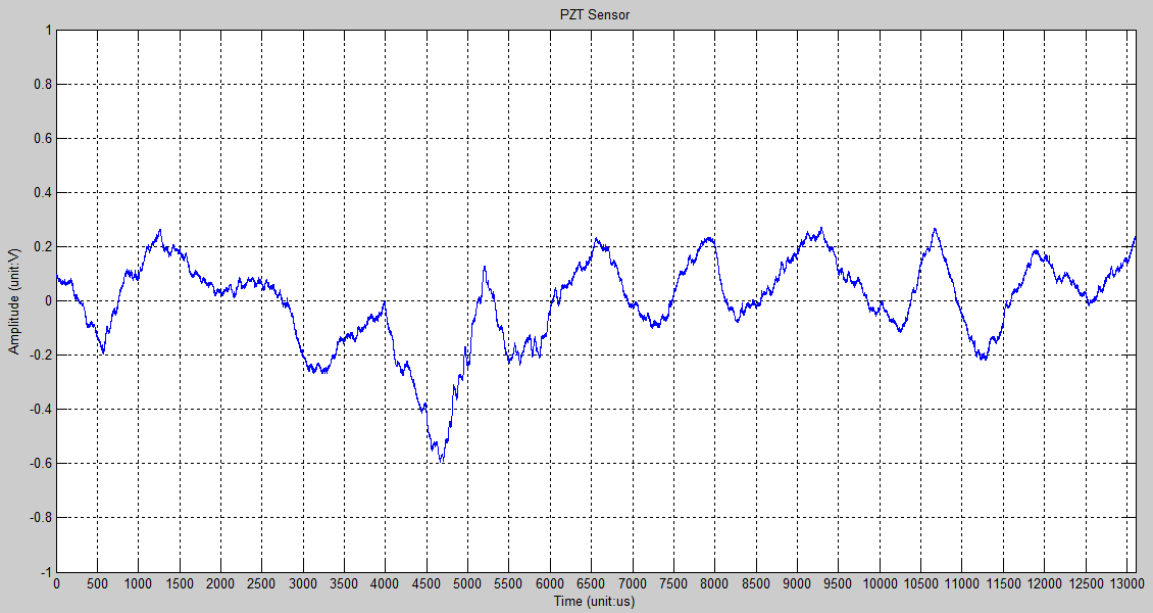

The signal from PZT sensor

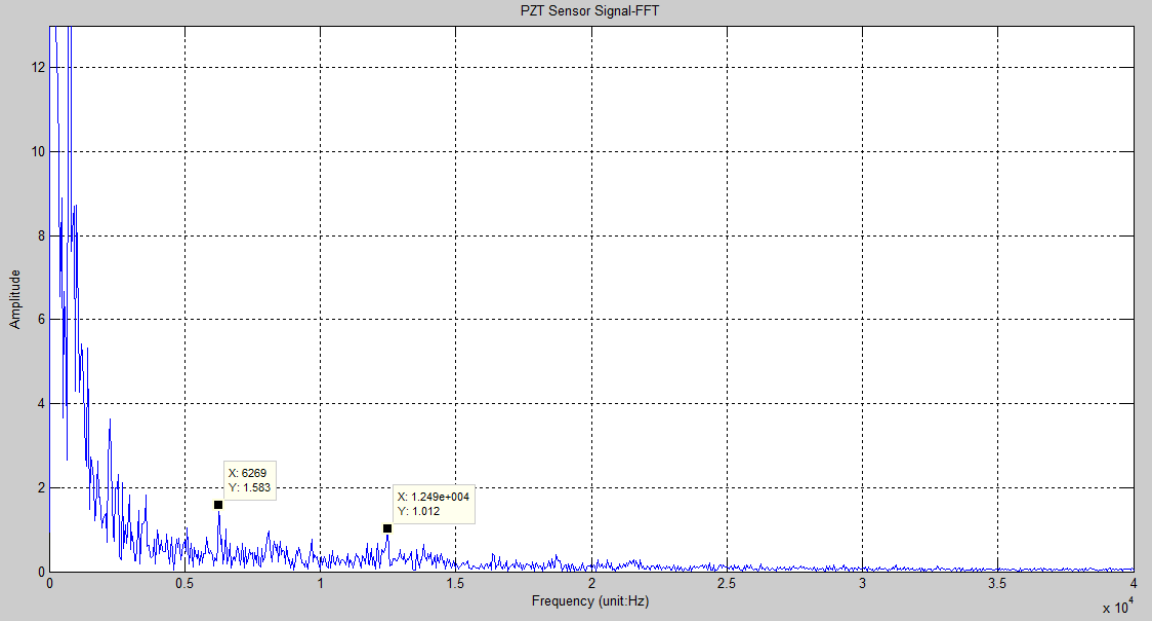

Figure A.19 - The FFT result of the PZT sensor's signal

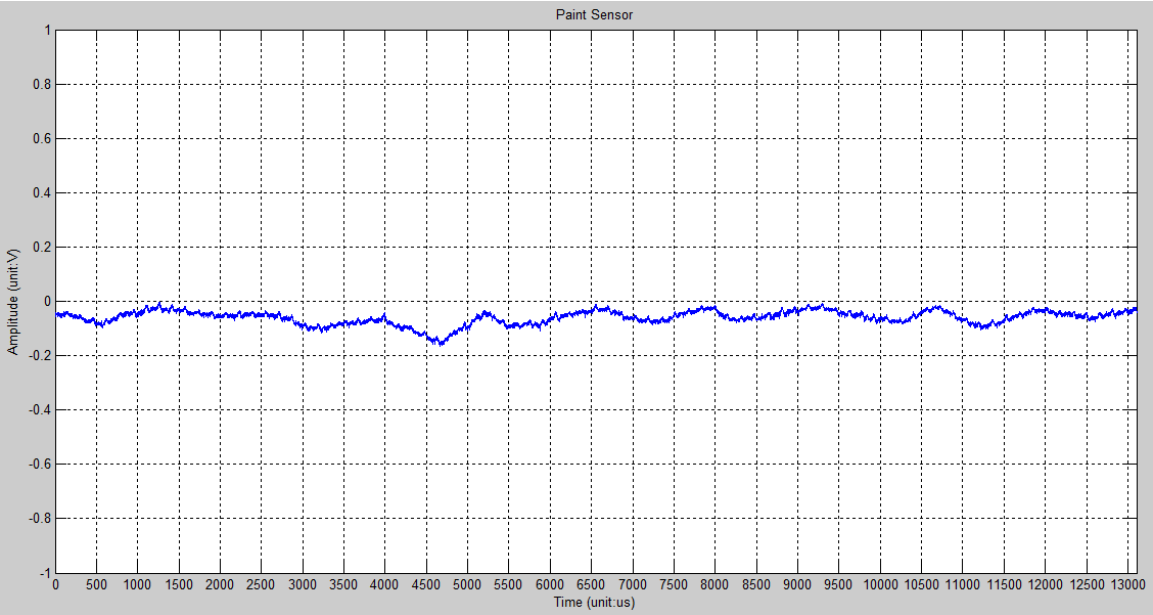

The signal from Paint sensor

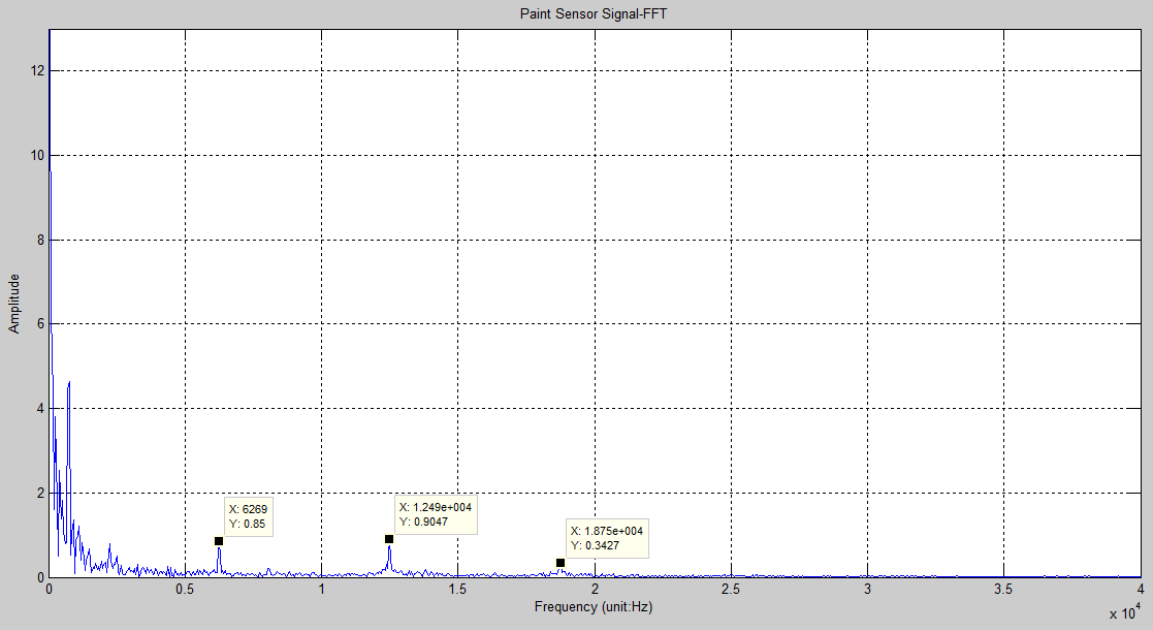

Figure A.20 - The FFT result of the Paint sensor's signal

2014-03-14 Test4 (Time: 13:32:12)

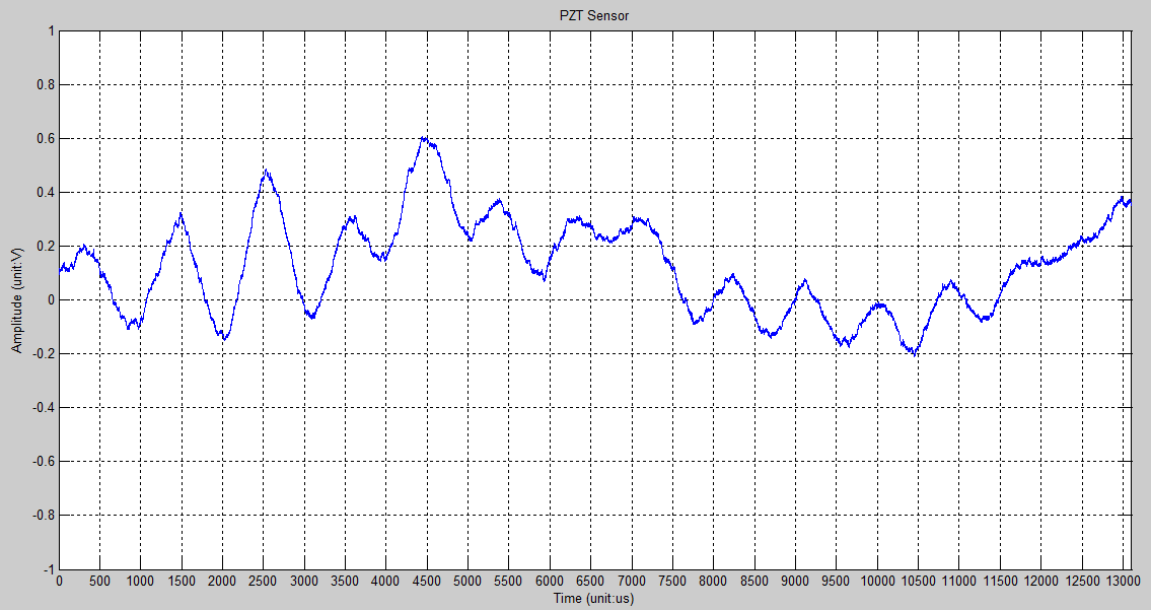

The signal from PZT sensor

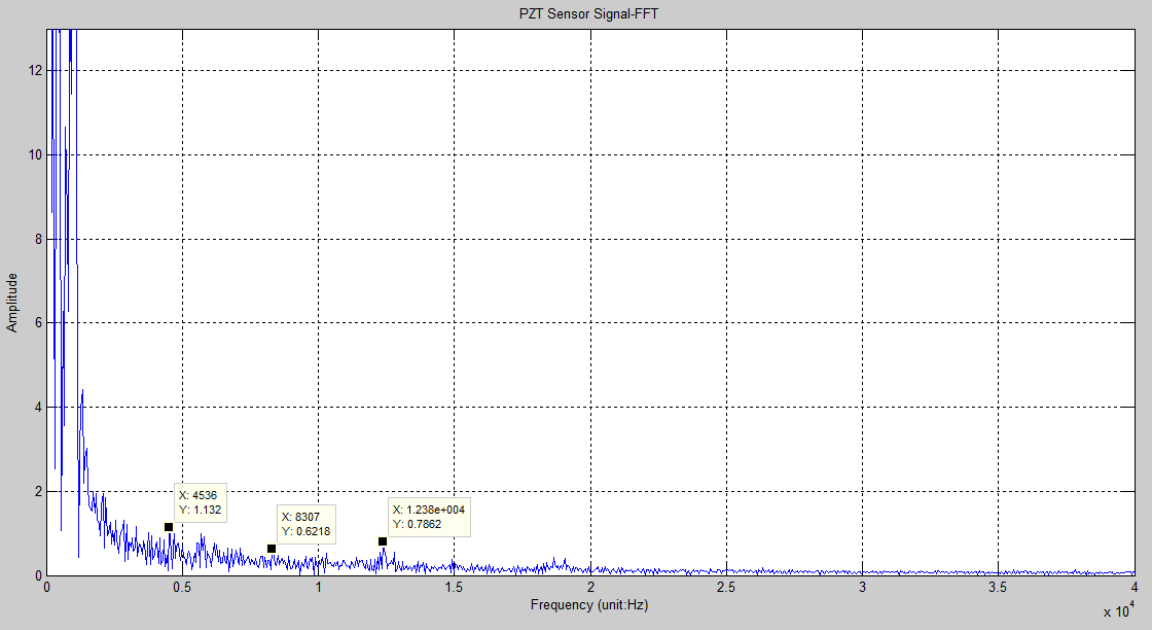

Figure A.21 - The FFT result of the PZT sensor's signal

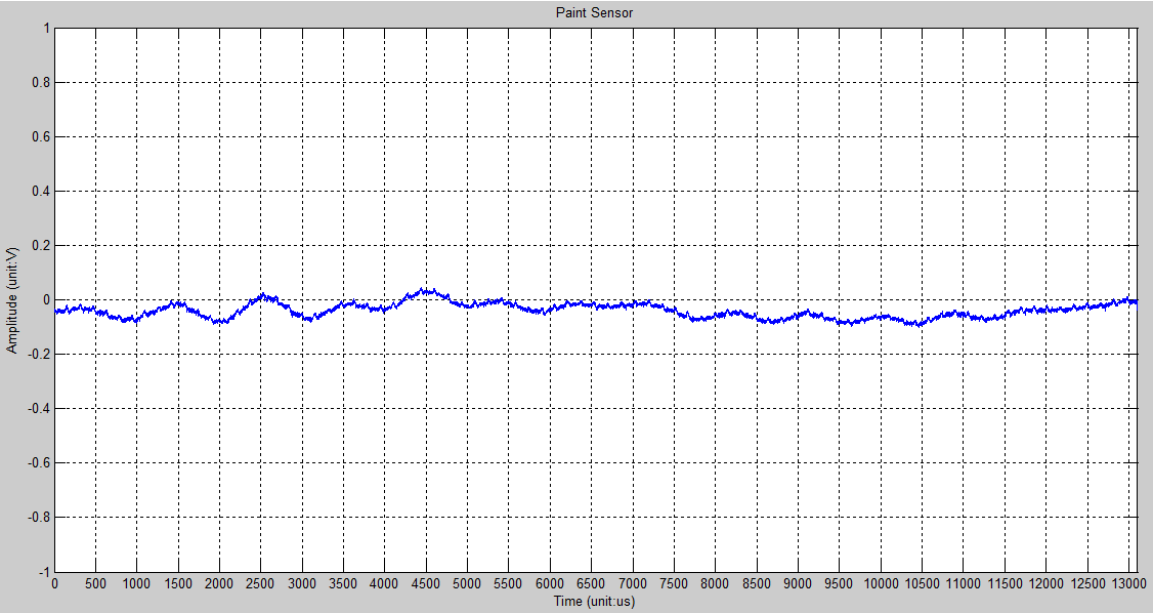

The signal from Paint sensor

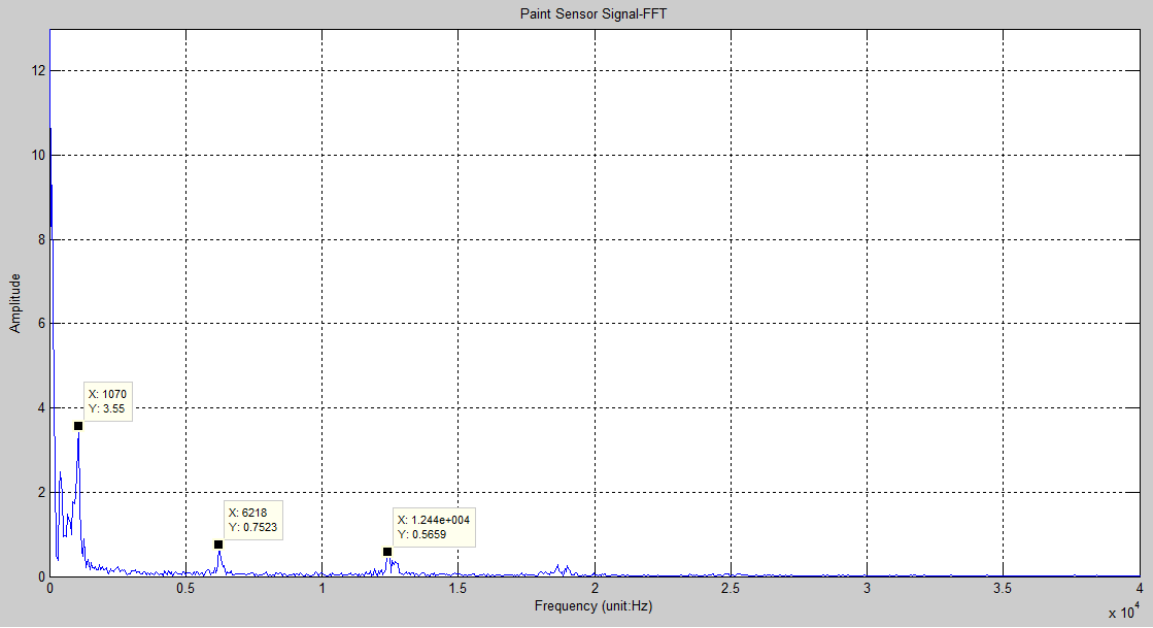

Figure A.22 - The FFT result of the Paint sensor's signal

2014-03-14 Test5 (Time: 13:39:07)

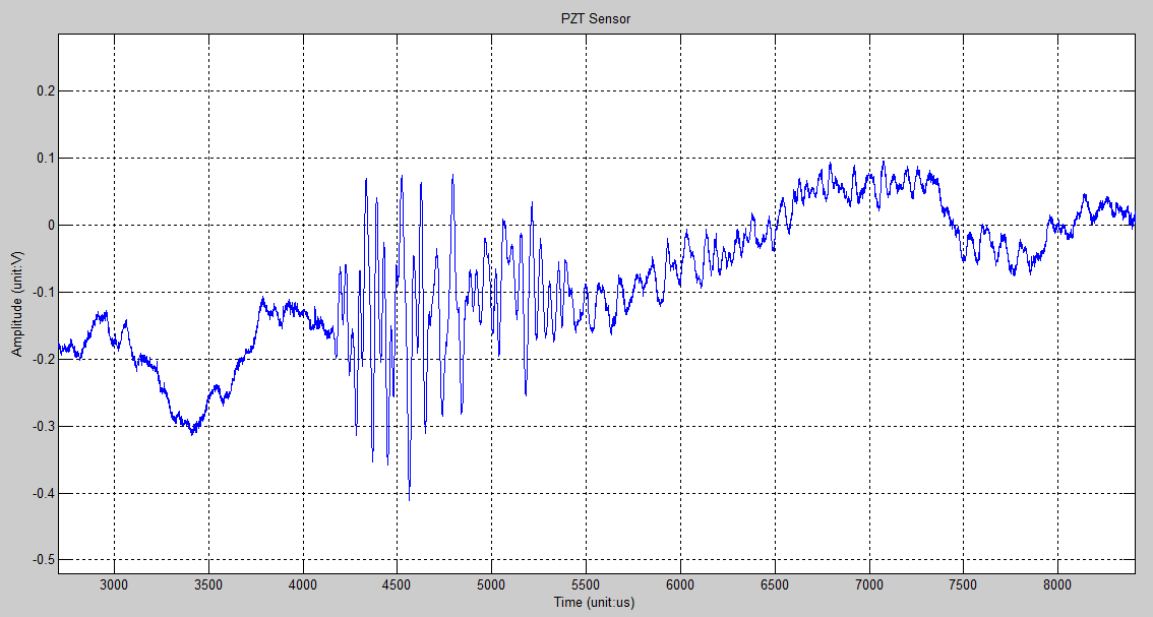

The signal from PZT sensor

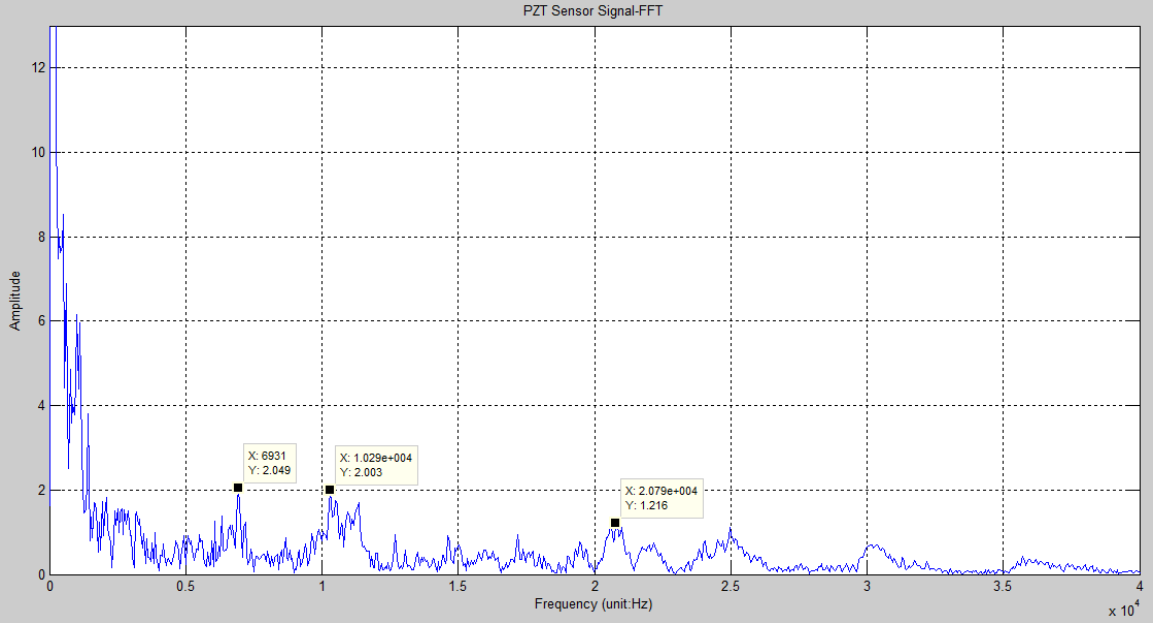

Figure A.23 - The FFT result of the PZT sensor's signal

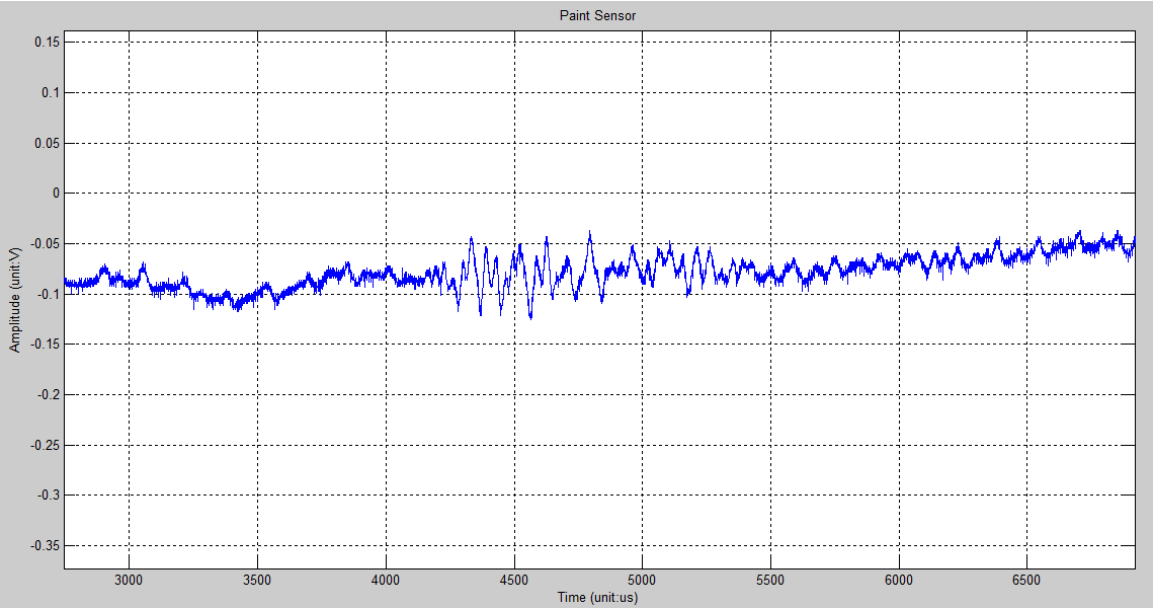

The signal from Paint sensor

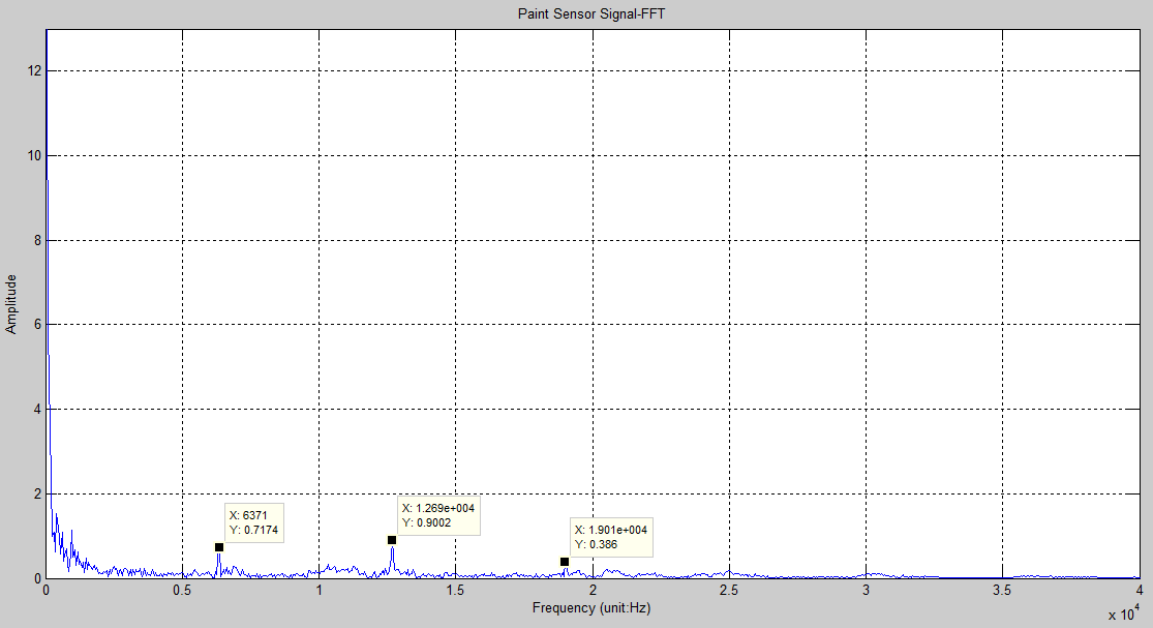

Figure A.24 - The FFT result of the Paint sensor's signal

2014-03-14 Test6 (Time: 13:47:36)

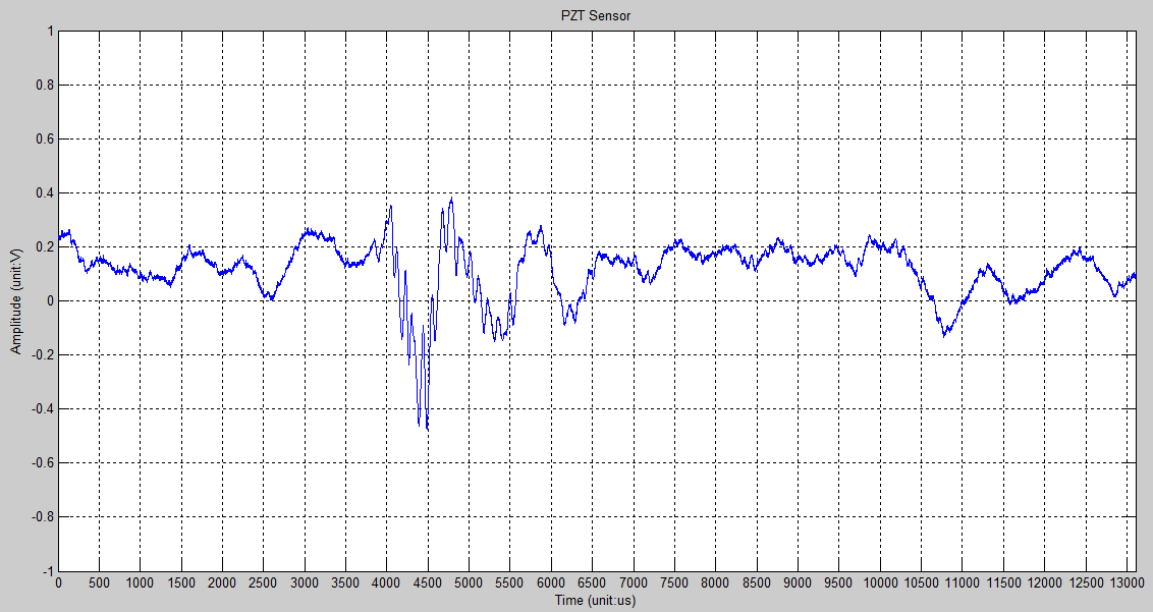

The signal from PZT sensor

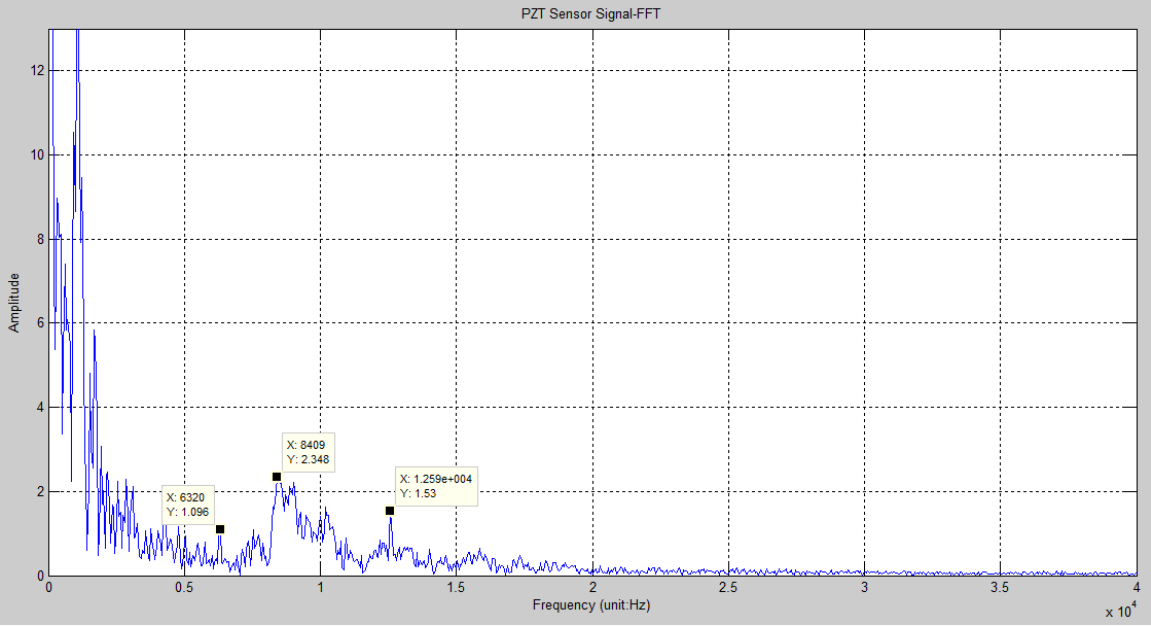

Figure A.25 - The FFT result of the PZT sensor's signal

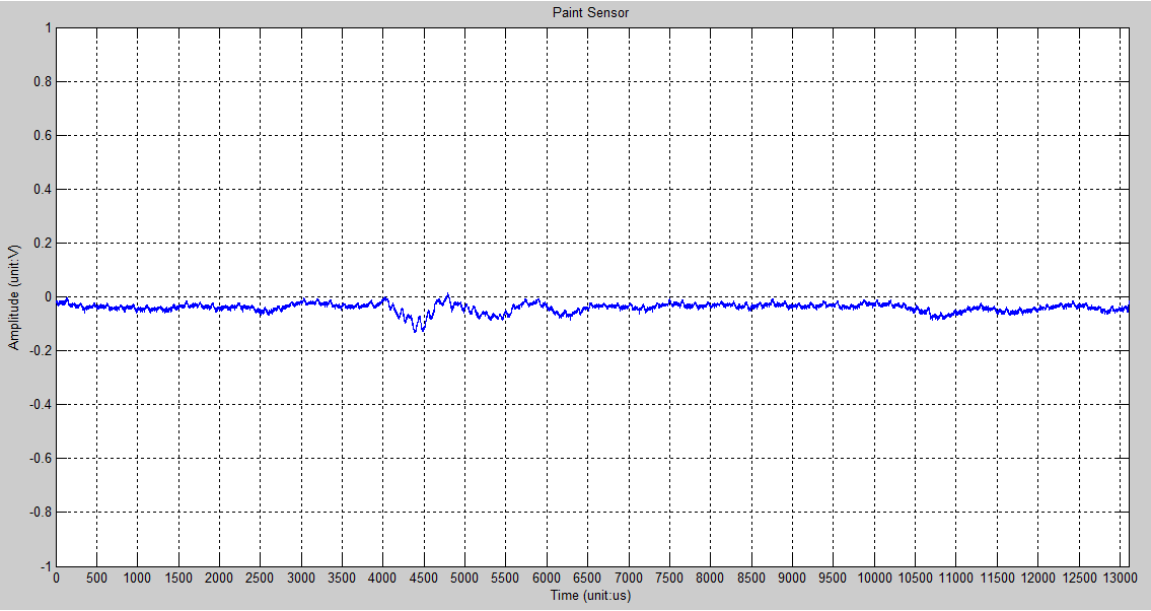

The signal from Paint sensor

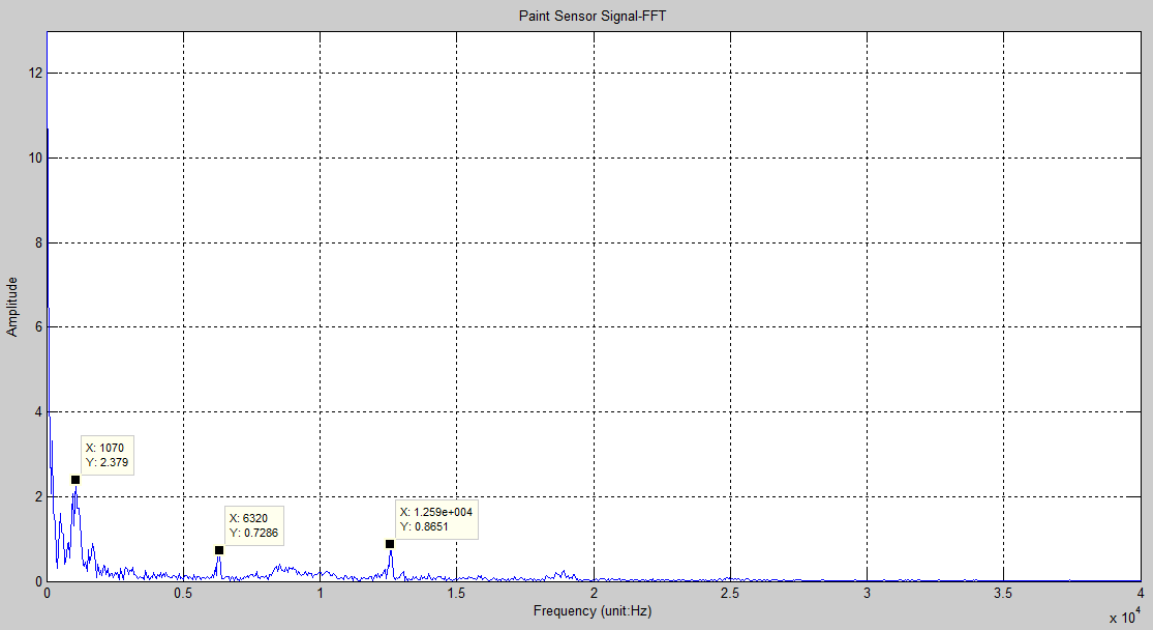

Figure A.26 - The FFT result of the Paint sensor's signal

2014-03-14 Test7 (Time: 13:55:36)

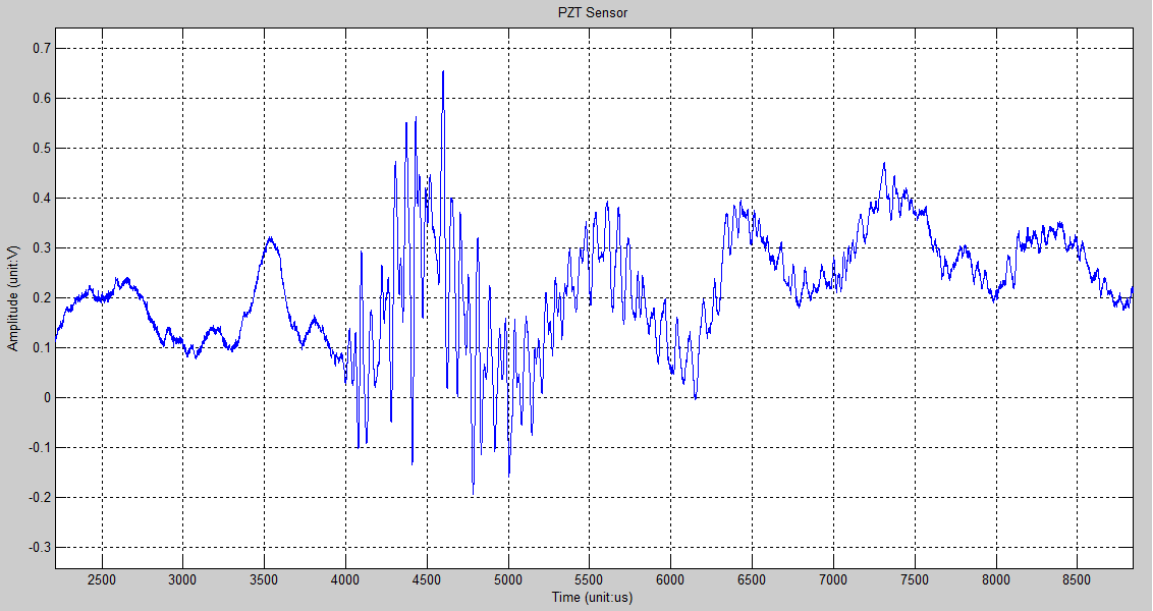

The signal from PZT sensor

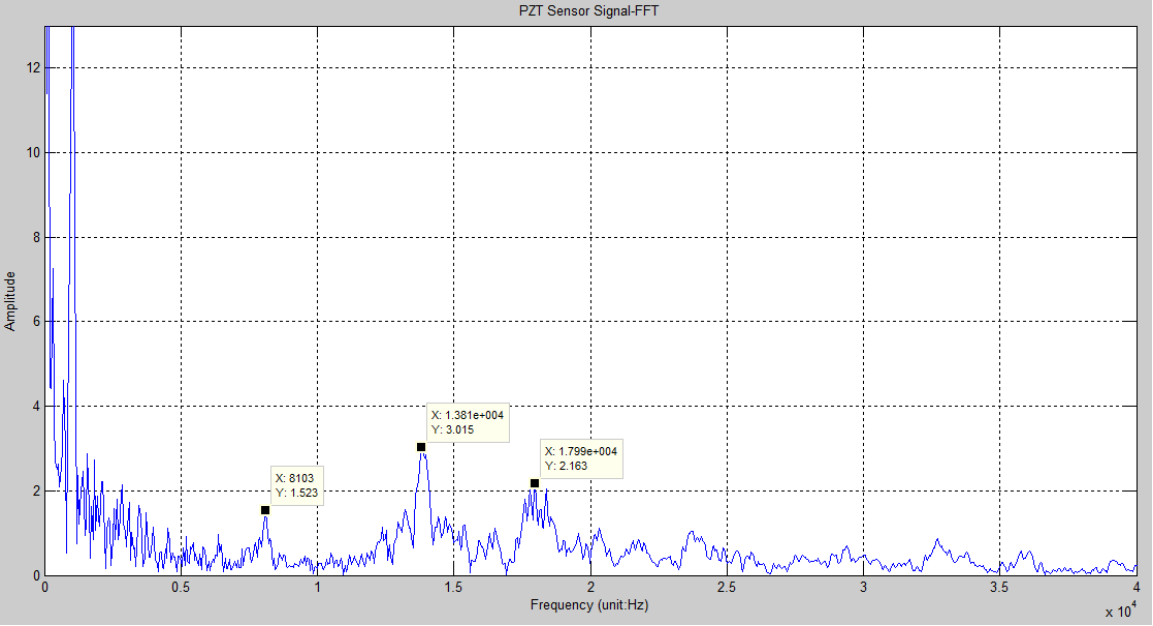

Figure A.27 - The FFT result of the PZT sensor's signal

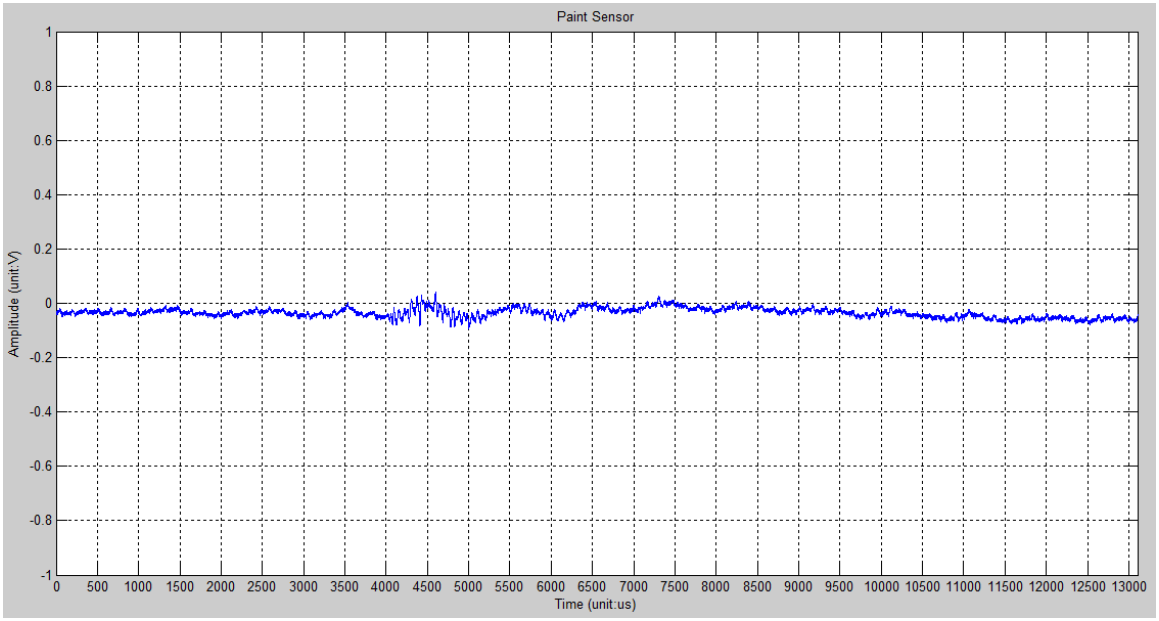

The signal from Paint sensor

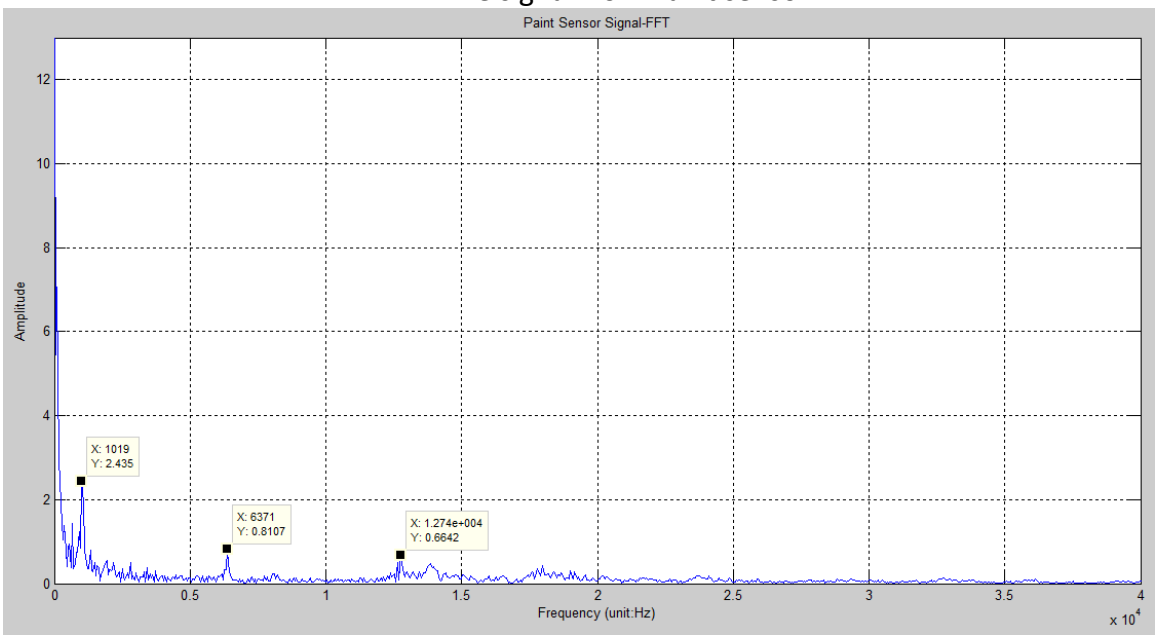

Figure A.28 - The FFT result of the Paint sensor's signal

2014-03-14 Test8 (Time: 13:59:13)

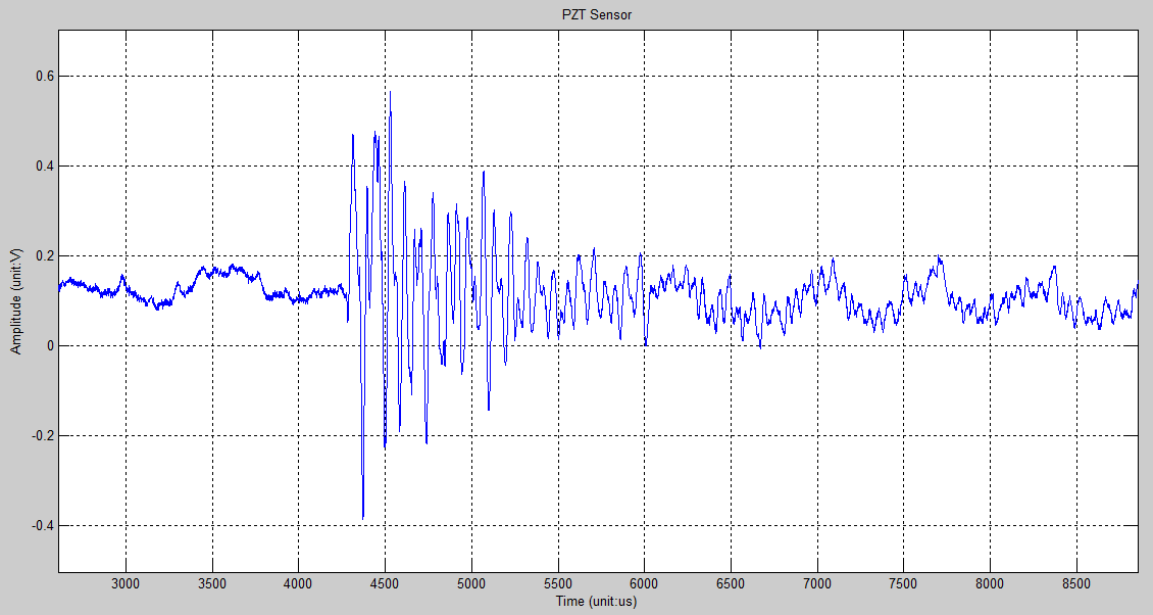

The signal from PZT sensor

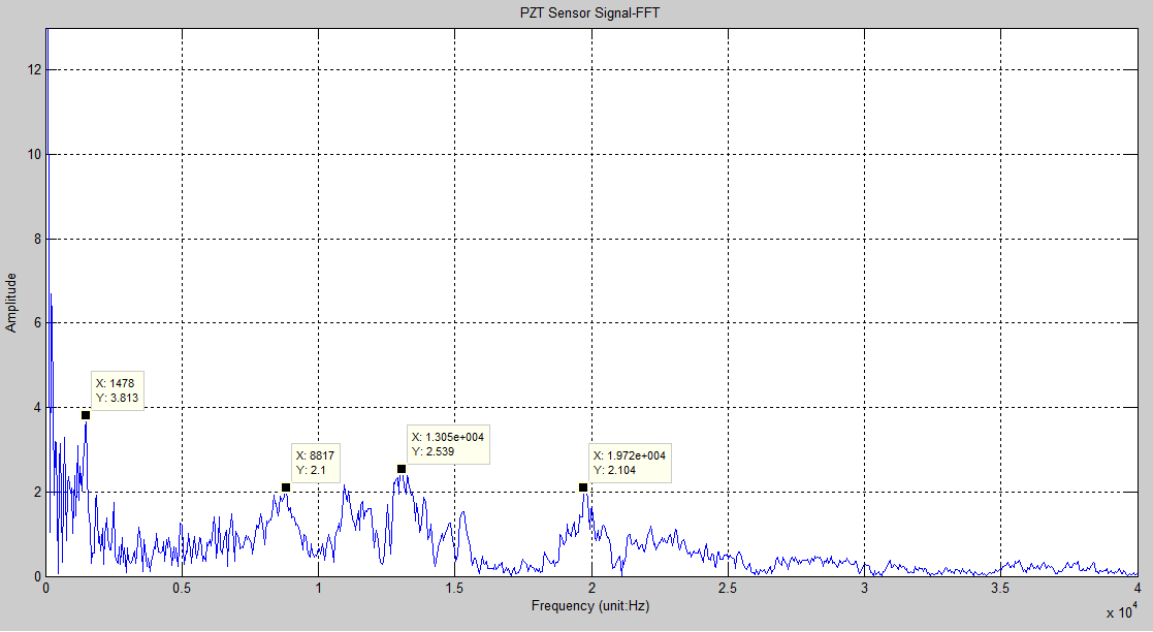

Figure A.29 - The FFT result of the PZT sensor's signal

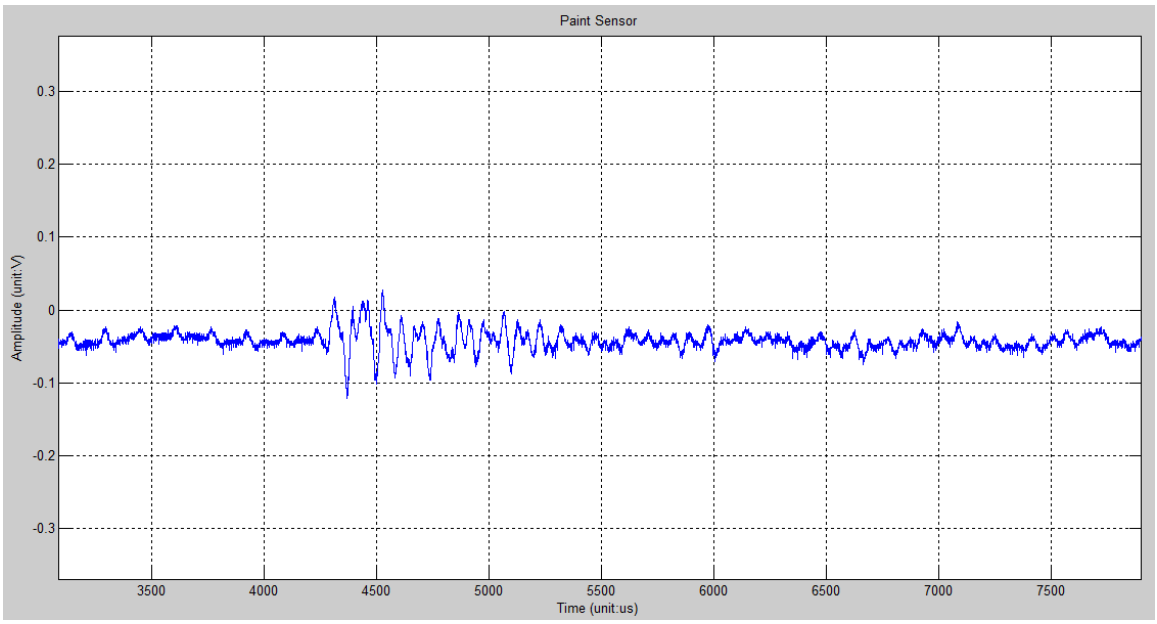

The signal from Paint sensor

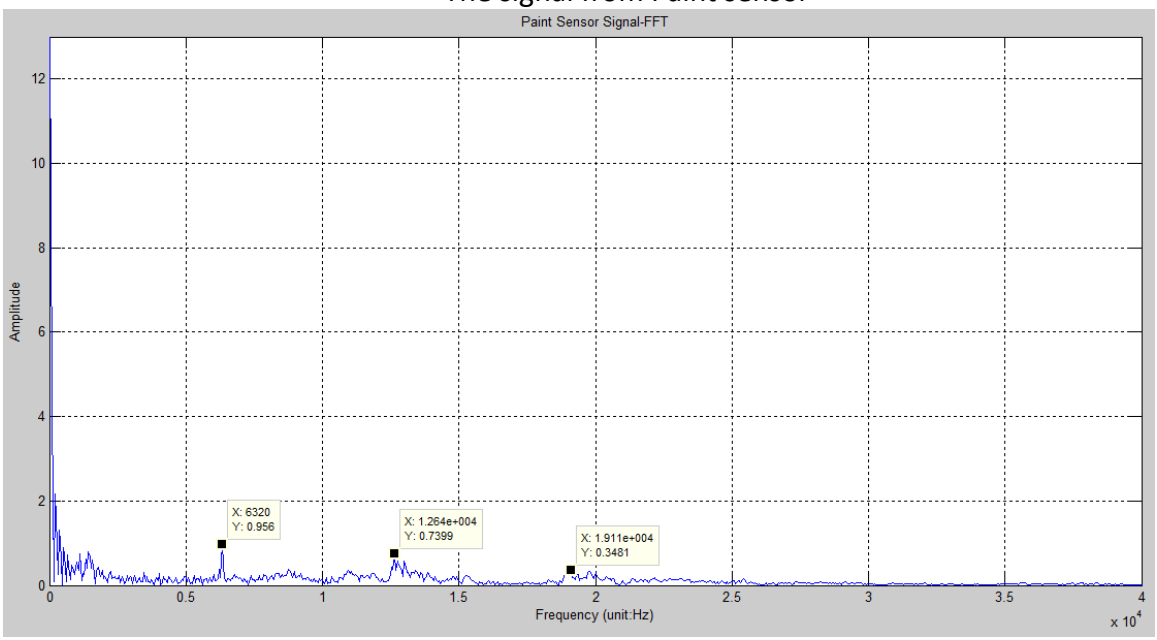

Figure A.30 - The FFT result of the Paint sensor's signal

2014-03-14 Test9 (Time: 14:18:07)

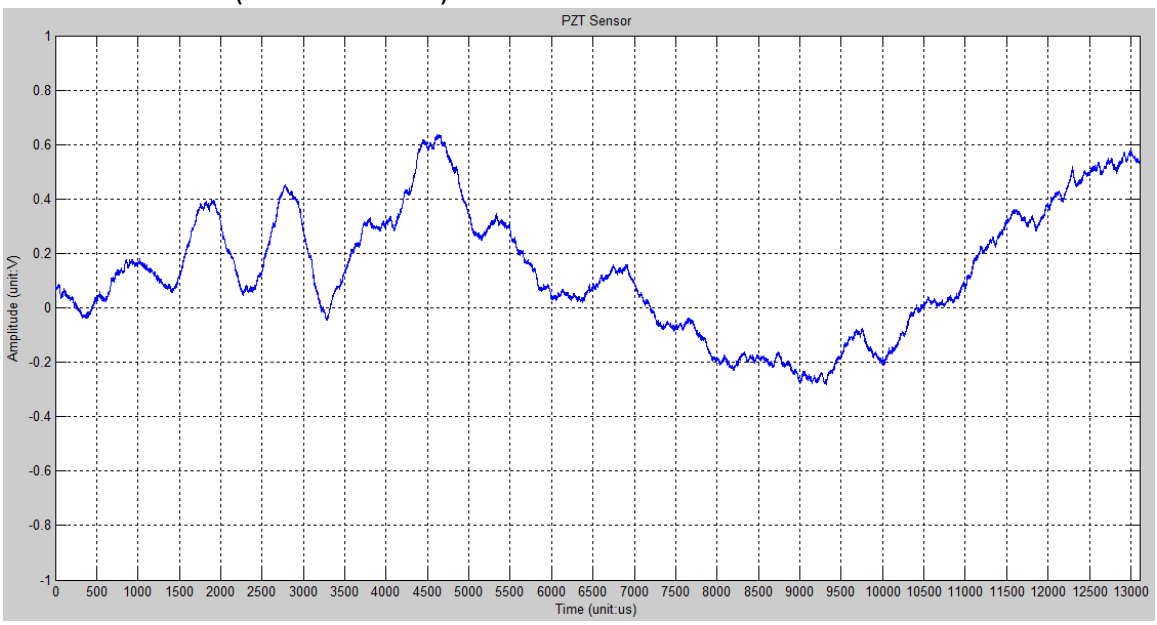

The signal from PZT sensor

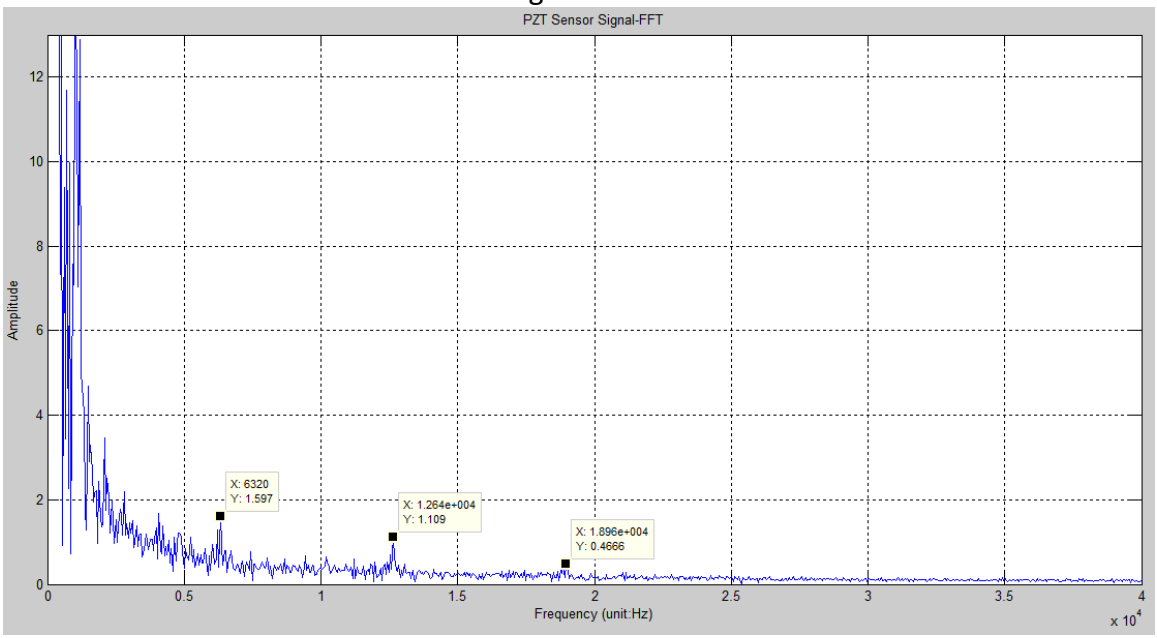

Figure A.31 - The FFT result of the PZT sensor's signal

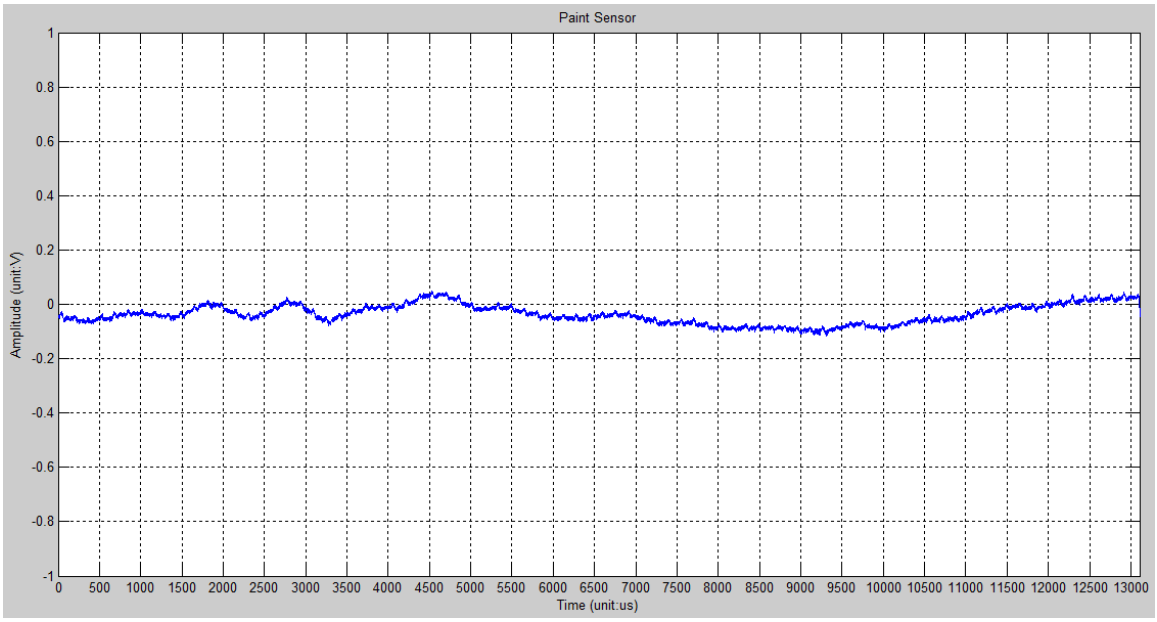

The signal from Paint sensor

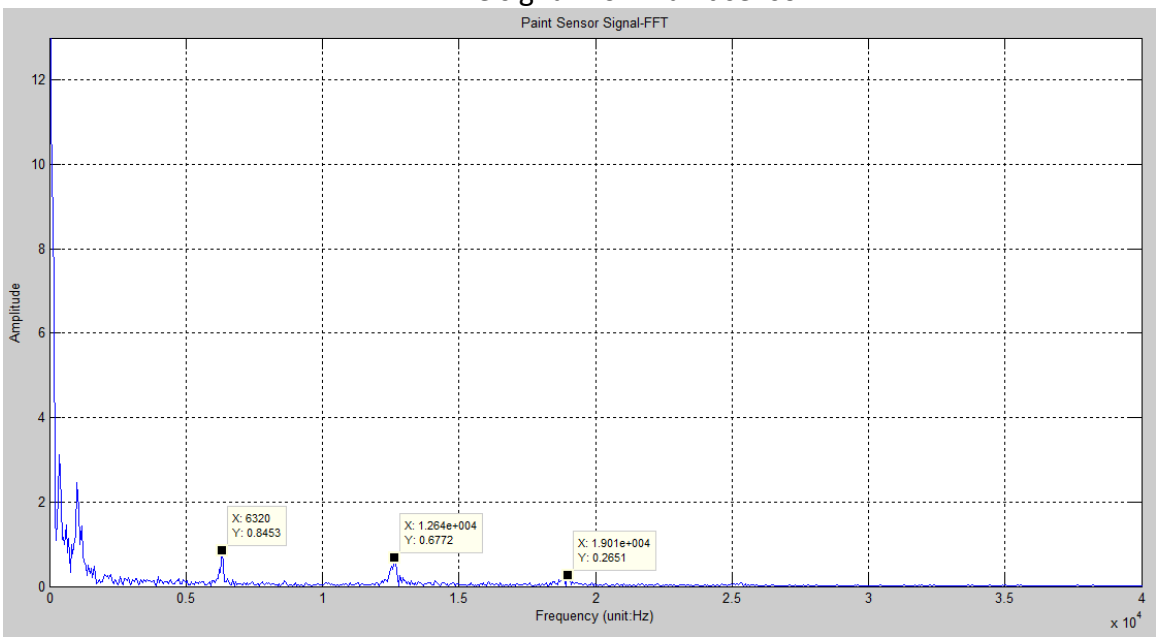

Figure A.32 - The FFT result of the Paint sensor's signal

2014-03-14 Test10 (Time: 14:25:15)

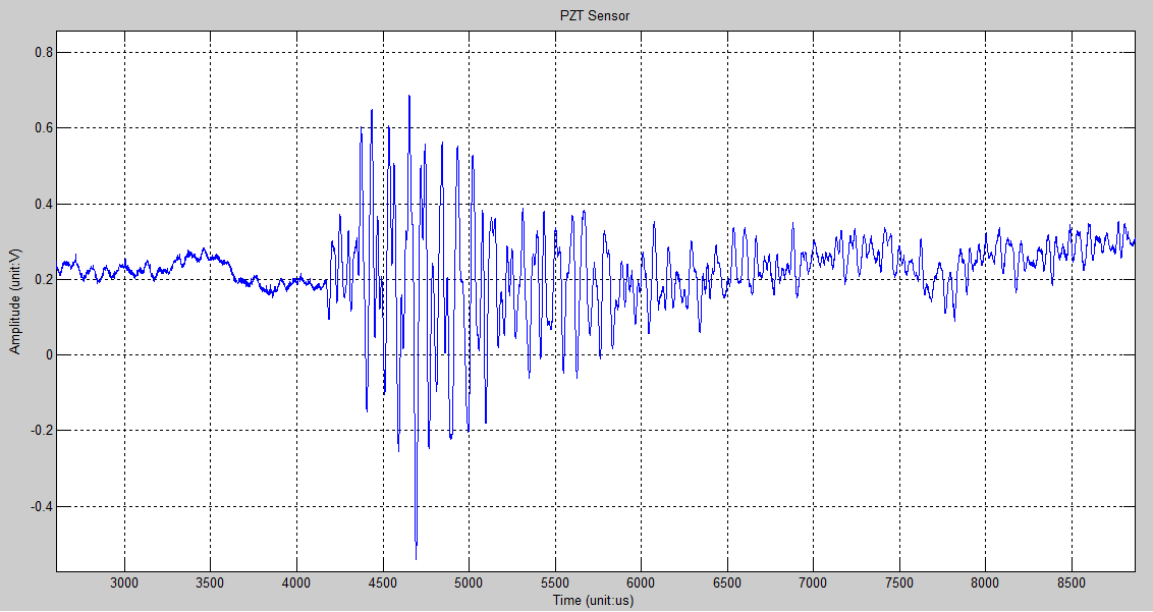

The signal from PZT sensor

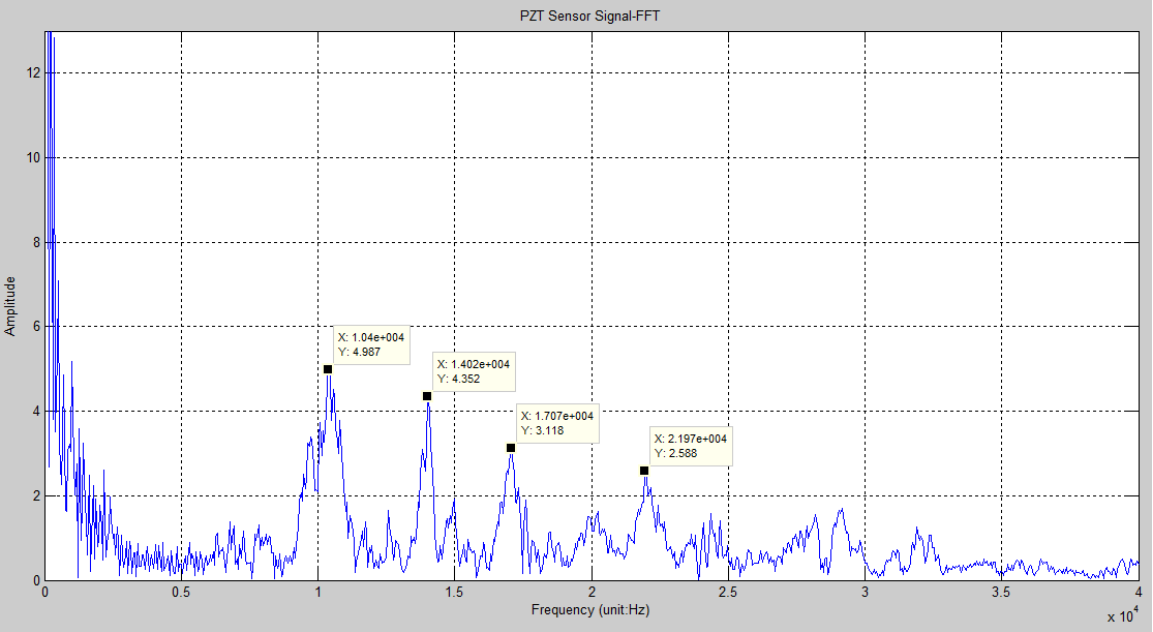

Figure A.33 - The FFT result of the PZT sensor's signal

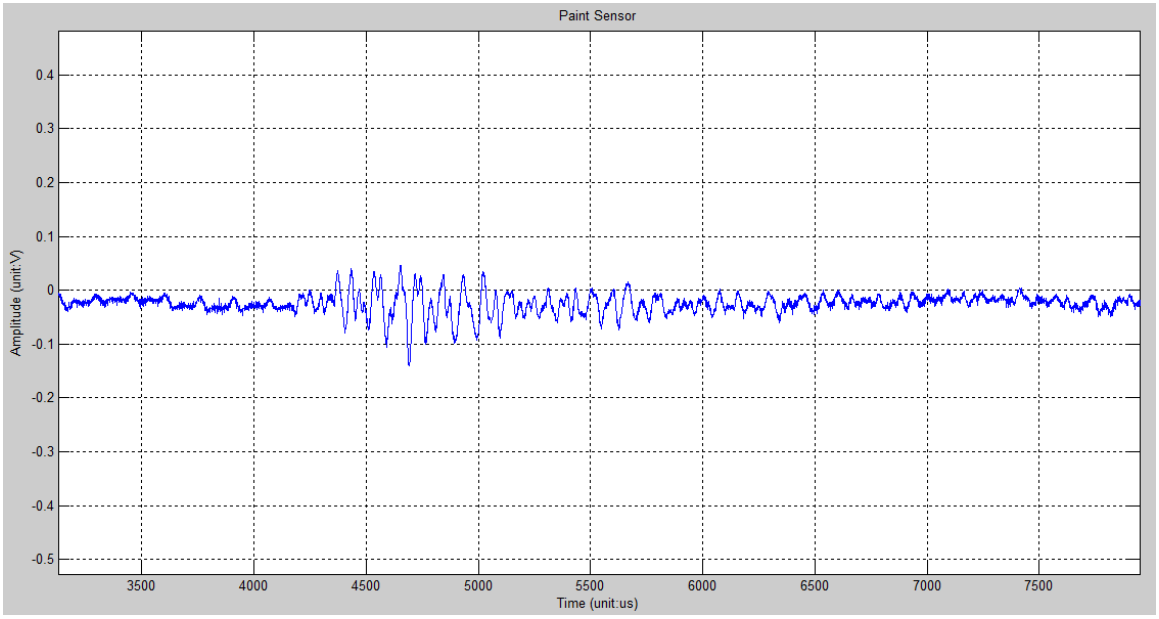

The signal from Paint sensor

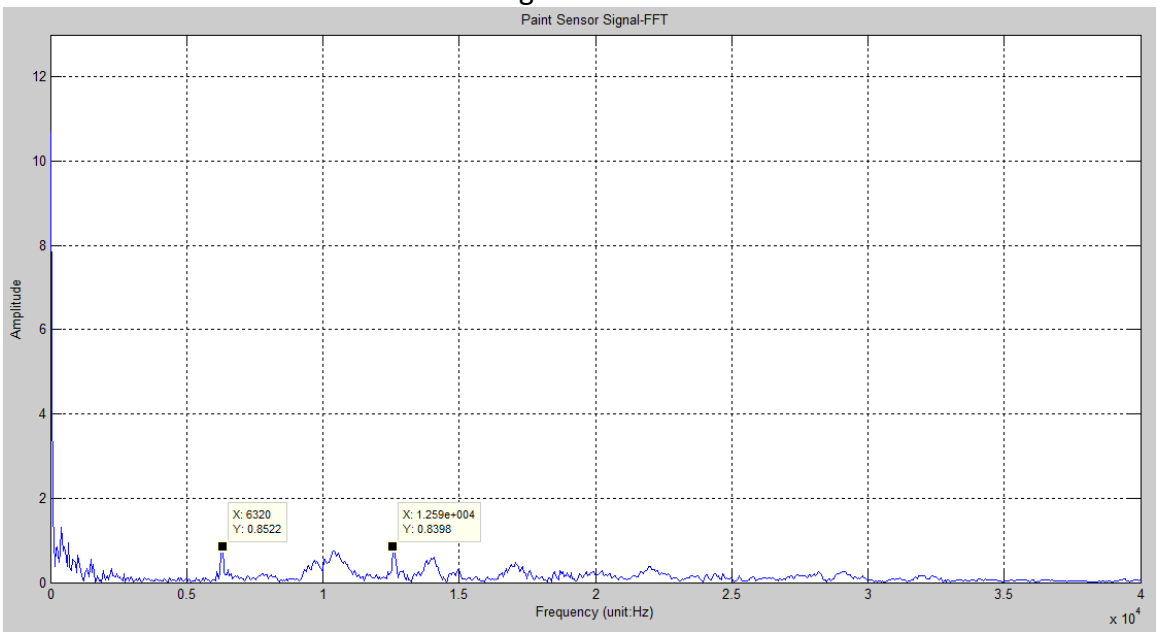

Figure A.34 - The FFT result of the Paint sensor's signal

2014-03-14 Test11 (Time: 14:29:50)

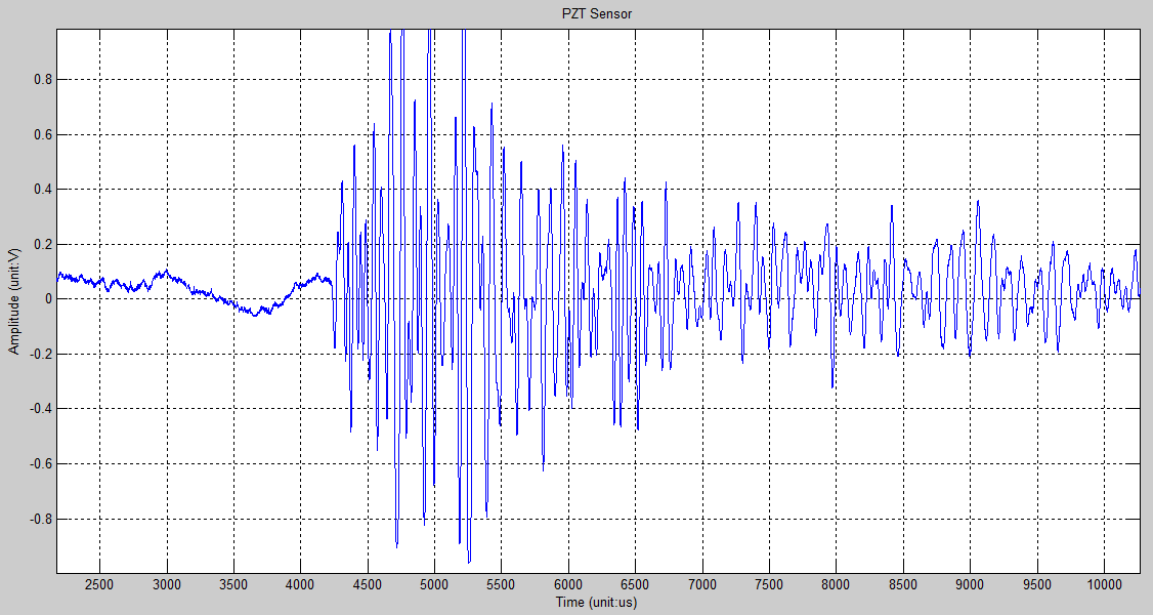

The signal from PZT sensor

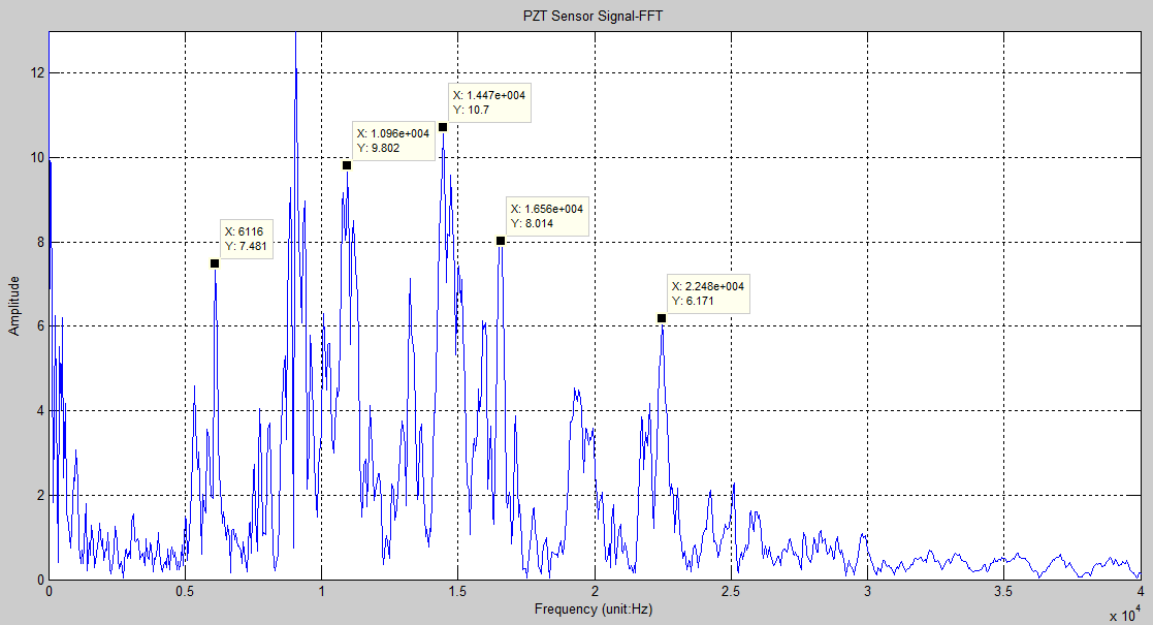

Figure A.35 - The FFT result of the PZT sensor's signal

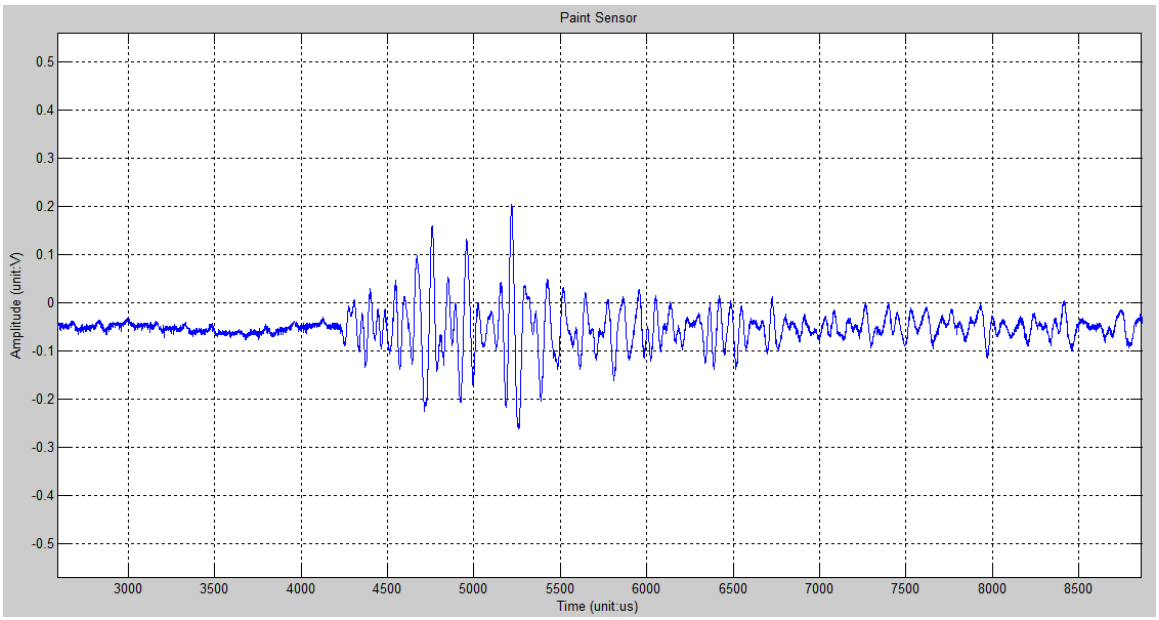

The signal from Paint sensor

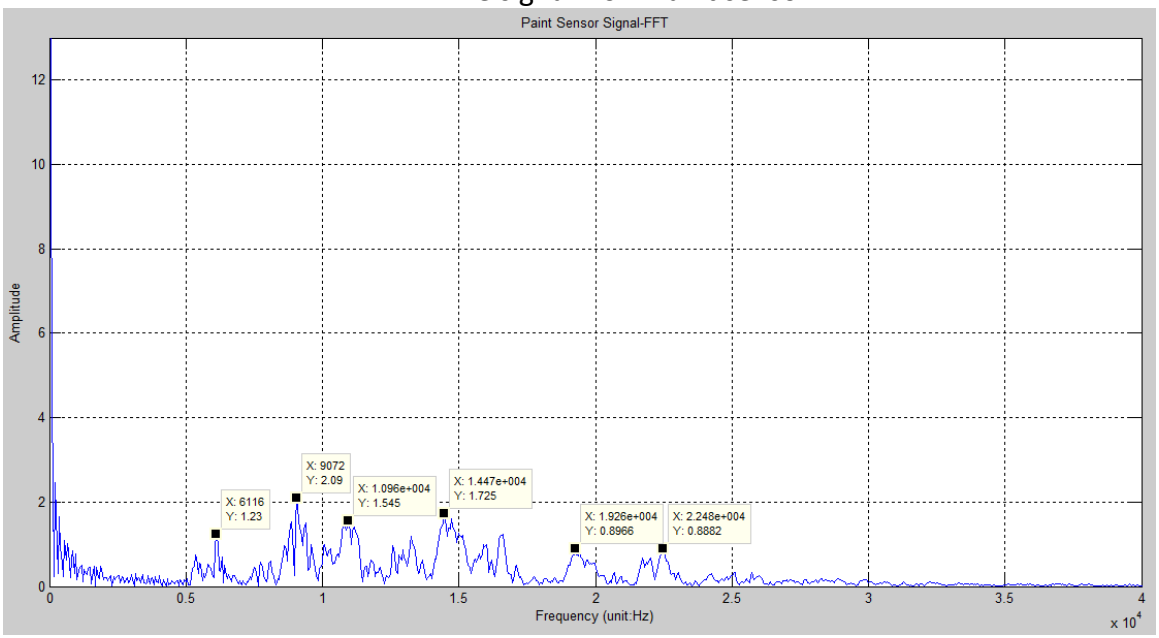

Figure A.36 - The FFT result of the Paint sensor's signal

2014-03-14 Test12 (Time: 14:34:07)

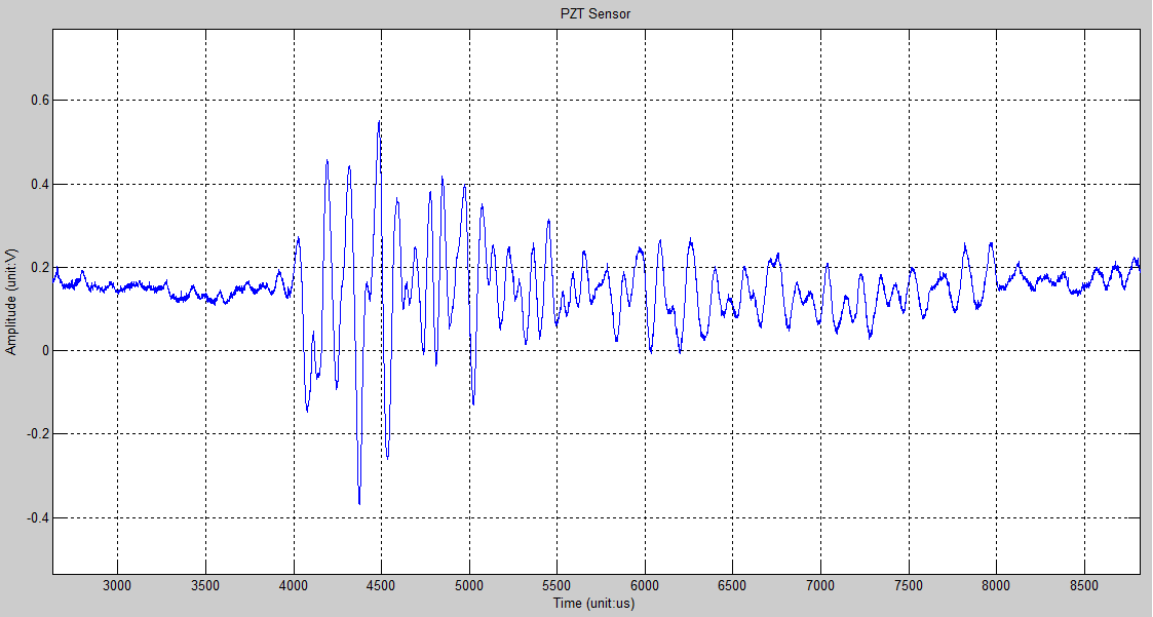

The signal from PZT sensor

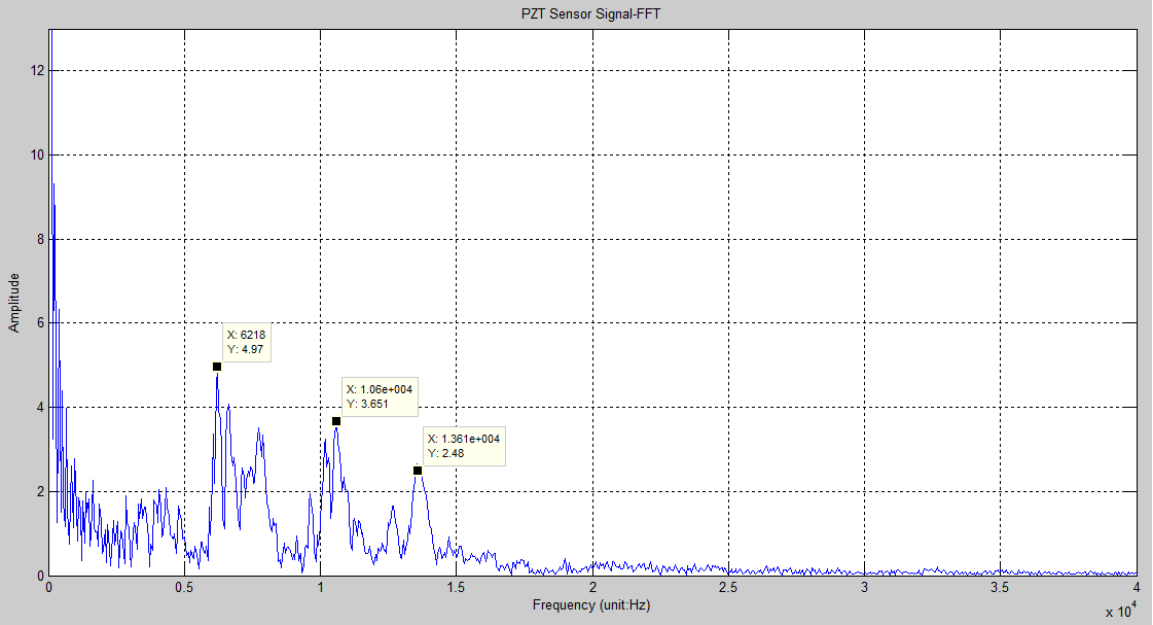

Figure A.37 - The FFT result of the PZT sensor's signal

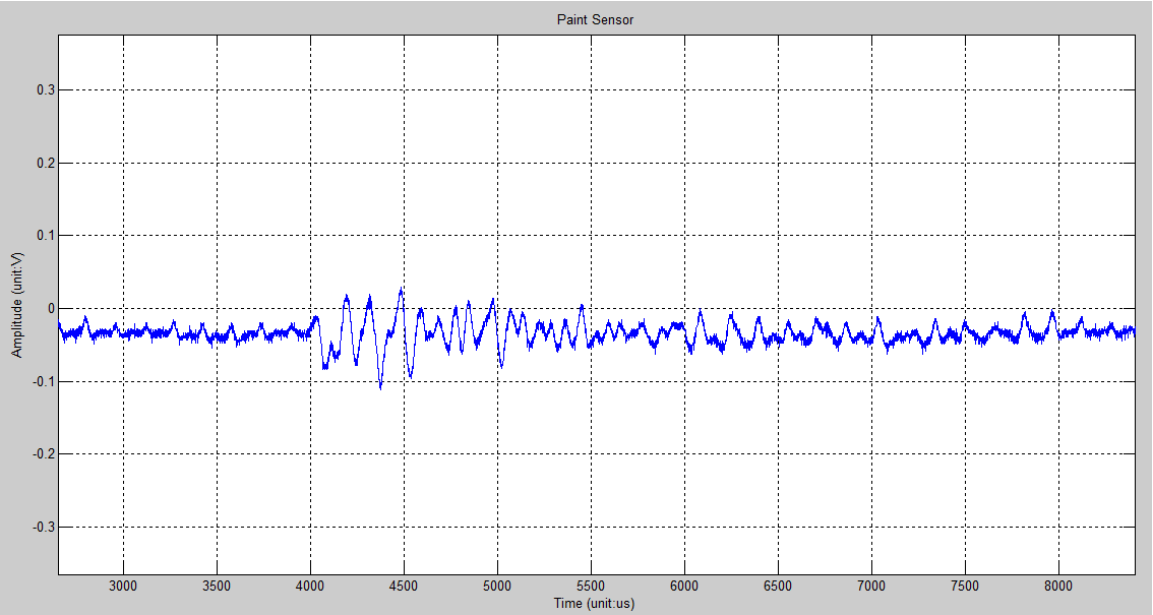

The signal from Paint sensor

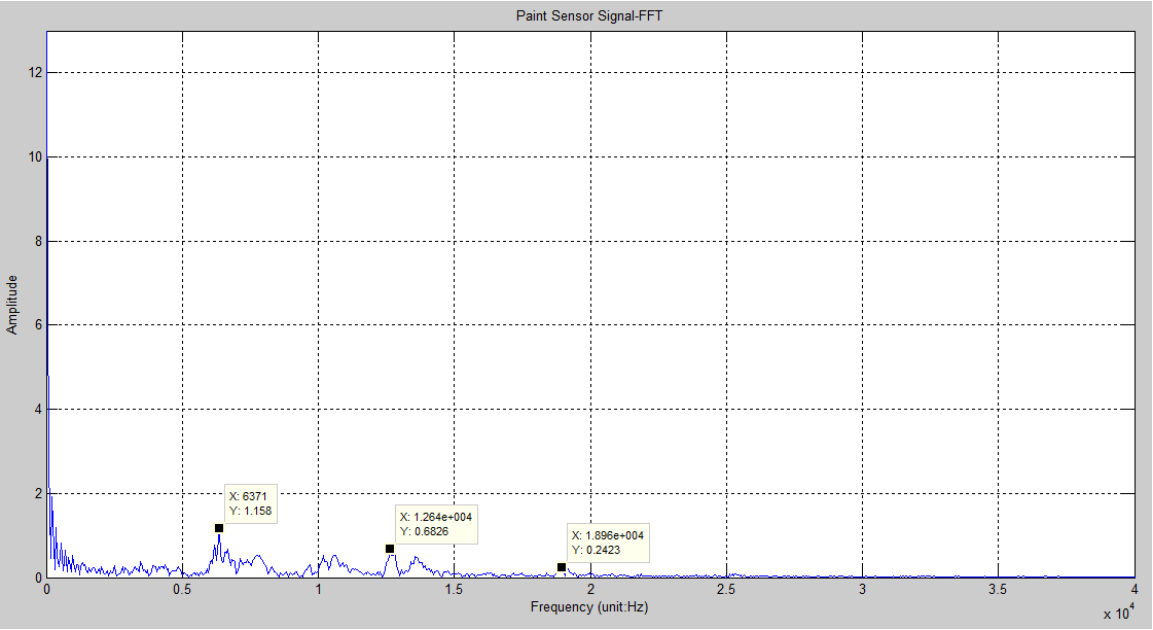

Figure A.38 - The FFT result of the Paint sensor's signal

Appendix B

Field Test Strain and Accelerameter Results
of
Bridge No.1619701 I-95 NB over Patuxent River

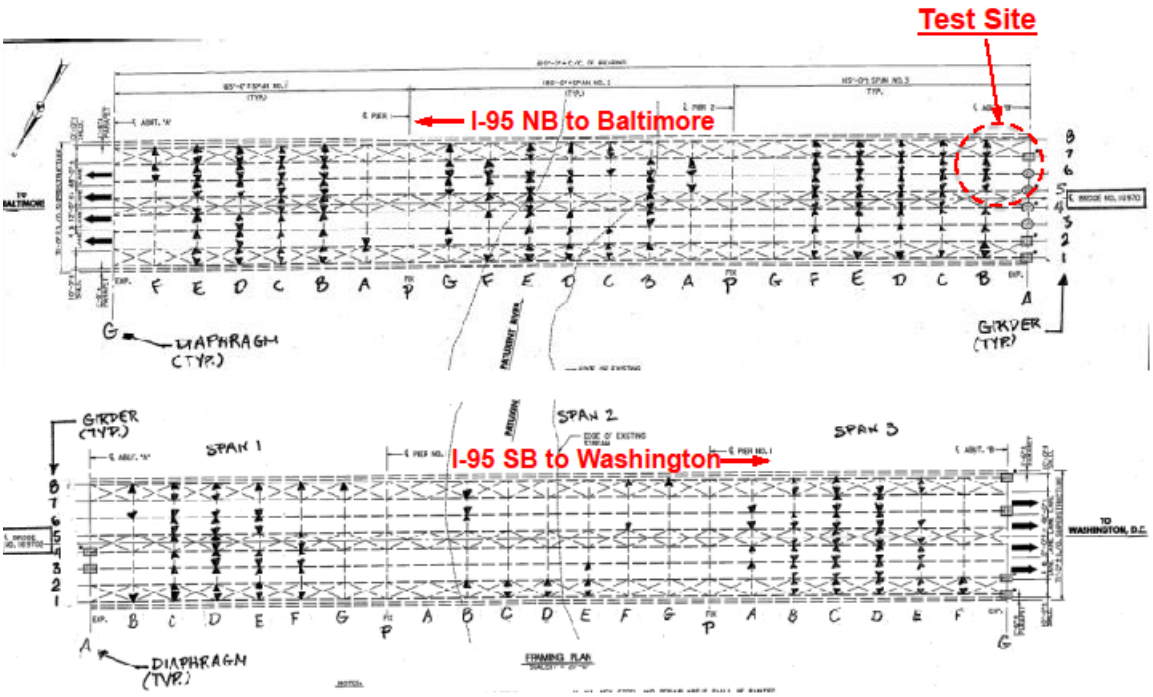

Figure B.1 – I95 Bridge testing site and sensor locations

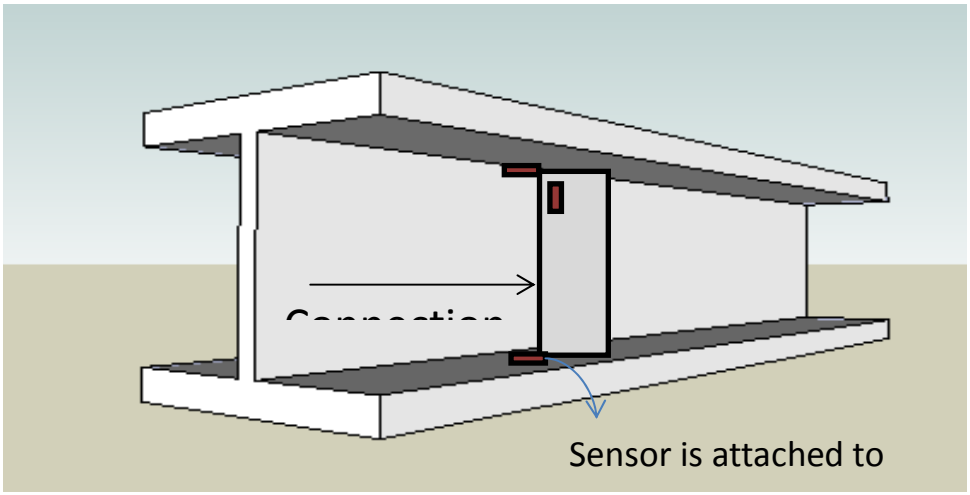

Figure B.2 – Schematic view of strain sensor locations

Table B.1 – Maximum stress ranges within test time ranges

Day , Time Range	Max Stress Range
03/11/2014, 5:02:54 PM - 7:38:36 PM	
Upper Flange	.93 ksi
Lower Flange	3.01 ksi
Connection Plate	1.52 ksi
03/12/2014, 11:06:24 AM - 12:05:15 PM	
Upper Flange	1.17 ksi
Lower Flange	3.92 ksi
Connection Plate	1.68 ksi
03/12/2014, 12:19:49 PM - 1:03:34 PM	
Upper Flange	1.21 ksi
Lower Flange	4.12 ksi
Connection Plate	1.88 ksi
03/14/2014, 12:24:40 PM - 1:06:29 PM	
Upper Flange	1.94 ksi
Lower Flange	4.01 ksi
Connection Plate	1.70 ksi
03/14/2014, 2:53:07 PM - 4:45:31PM	
Upper Flange	.94 ksi
Lower Flange	3.05 ksi
Connection Plate	1.83 ksi

Location Day	Start Time	End Time	Max Stress Range
Upper Flange			
03-11-2014	5:02:54 PM	7:38:36 PM	.93 ksi
03-12-2014	11:06:24 AM	12:05:15 PM	1.17 ksi
03-12-2014	12:19:49 PM	1:03:34 PM	1.21 ksi
03-14-2014	12:24:40 PM	1:06:29 PM	1.94 ksi
03-14-2014	2:53:07 PM	4:45:31PM	.94 ksi
Lower Flange			
03-11-2014	5:02:54 PM	7:38:36 PM	3.01 ksi
03-12-2014	11:06:24 AM	12:05:15 PM	3.92 ksi
03-12-2014	12:19:49 PM	1:03:34 PM	4.12 ksi
03-14-2014	12:24:40 PM	1:06:29 PM	4.01 ksi
03-14-2014	2:53:07 PM	4:45:31PM	3.05 ksi
Connection Plate			
03-11-2014	5:02:54 PM	7:38:36 PM	1.52 ksi
03-12-2014	11:06:24 AM	12:05:15 PM	1.68 ksi
03-12-2014	12:19:49 PM	1:03:34 PM	1.88 ksi
03-14-2014	12:24:40 PM	1:06:29 PM	1.70 ksi
03-14-2014	2:53:07 PM	4:45:31PM	1.83 ksi

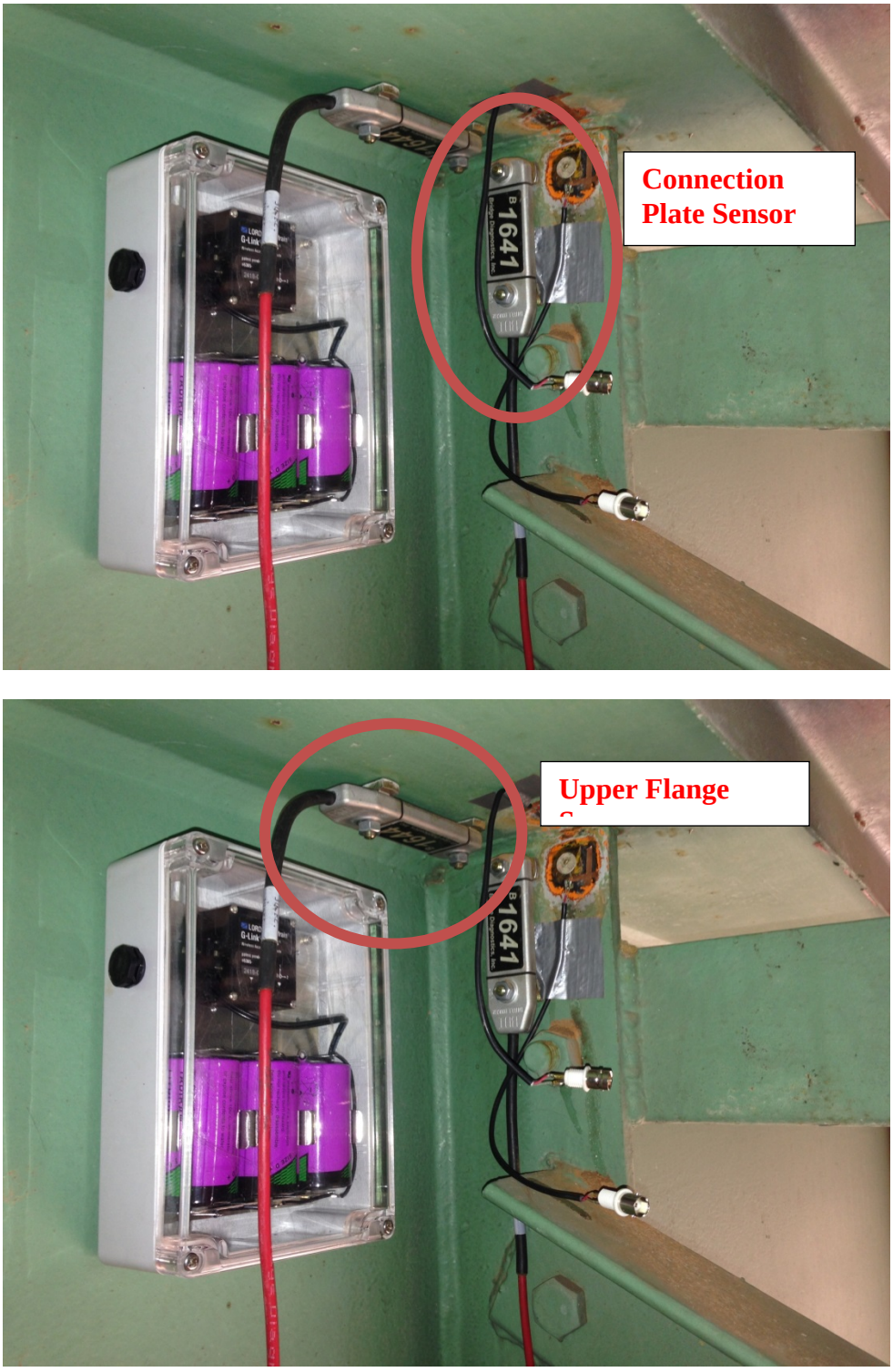

Figure B.3 – Wireless strain sensor placement on (a) the connection plate and (b) the top flange

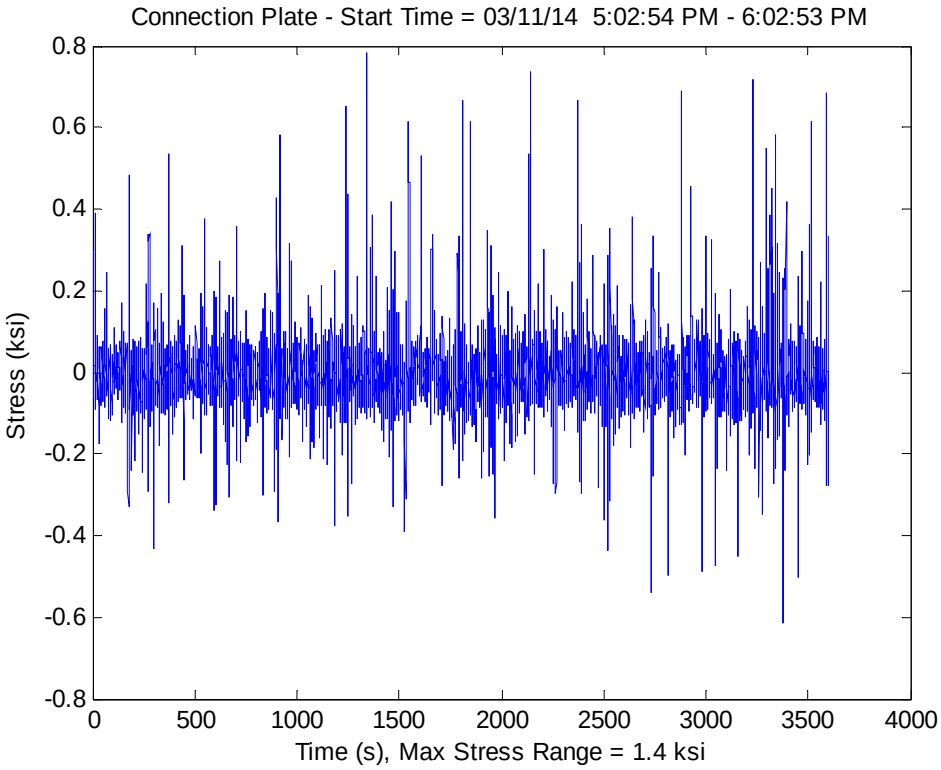

Figure B.4 – Sampling strain sensor data of the connection plate

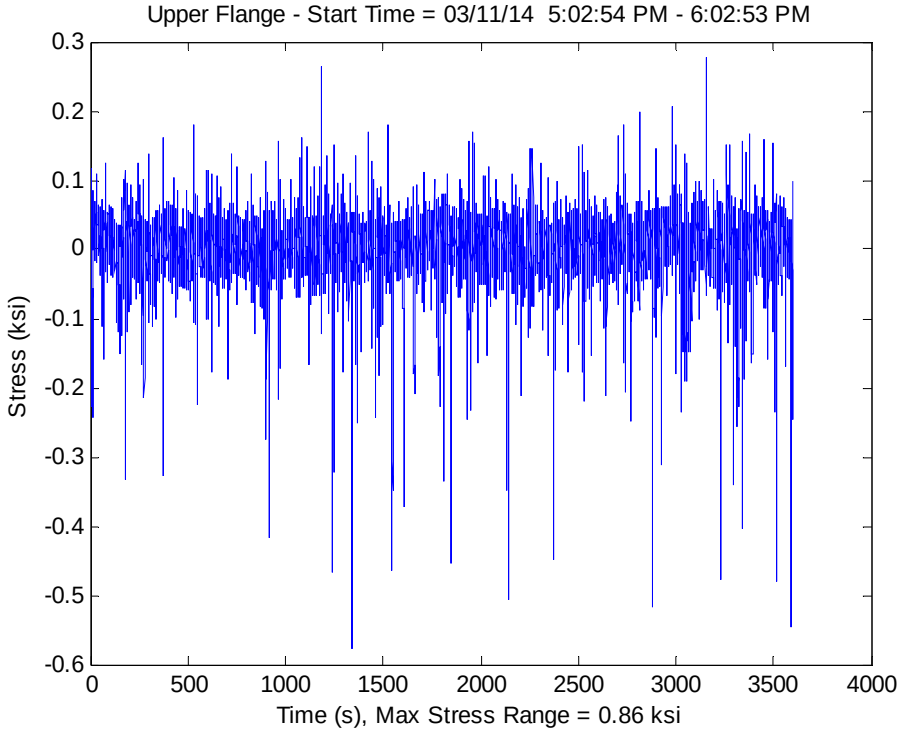

Figure B.5 – Sampling strain sensor data of the top flange

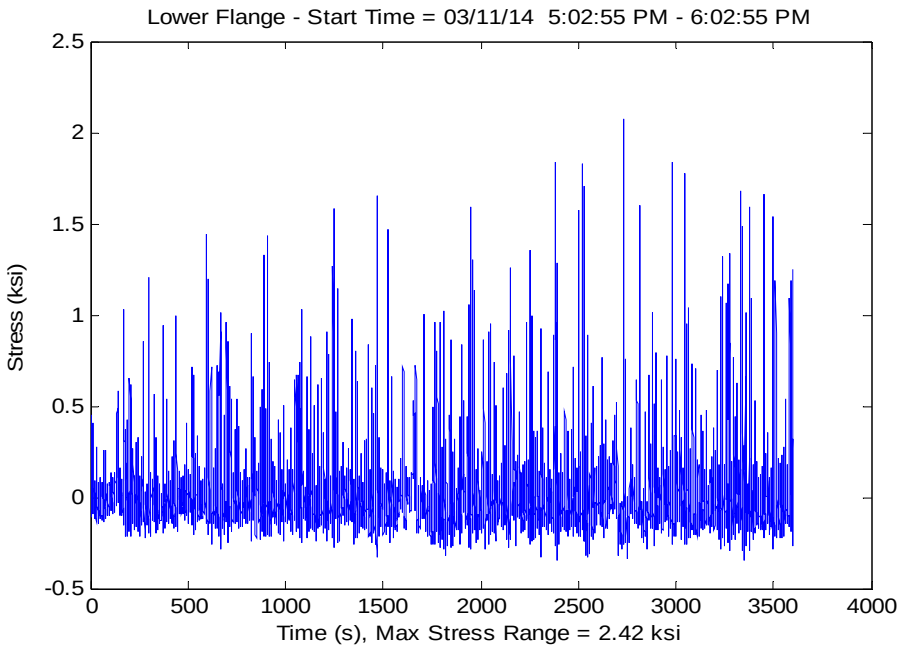

Figure B.6 – Sampling strain sensor data of the lower flange

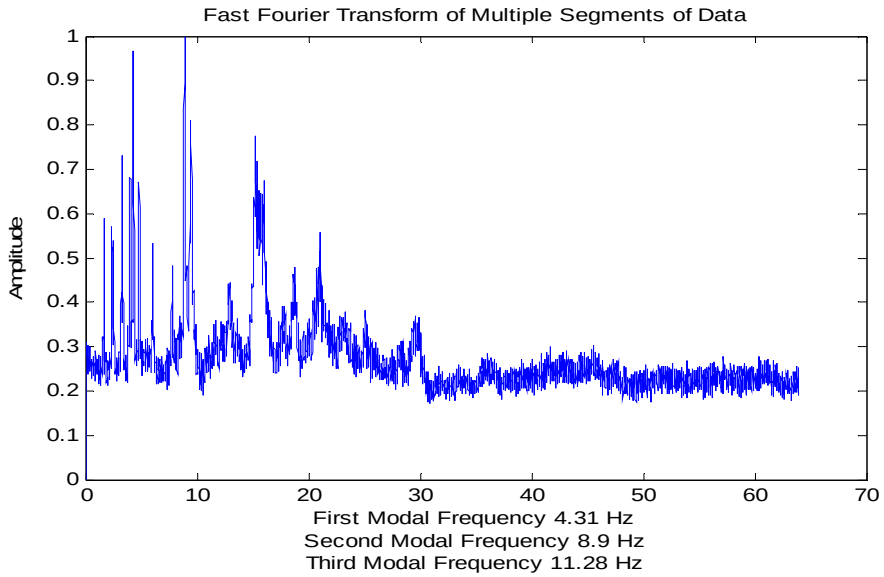

Figure B.7 – FFT of accelerometer data (11:24:40AM, 3/14/2014)

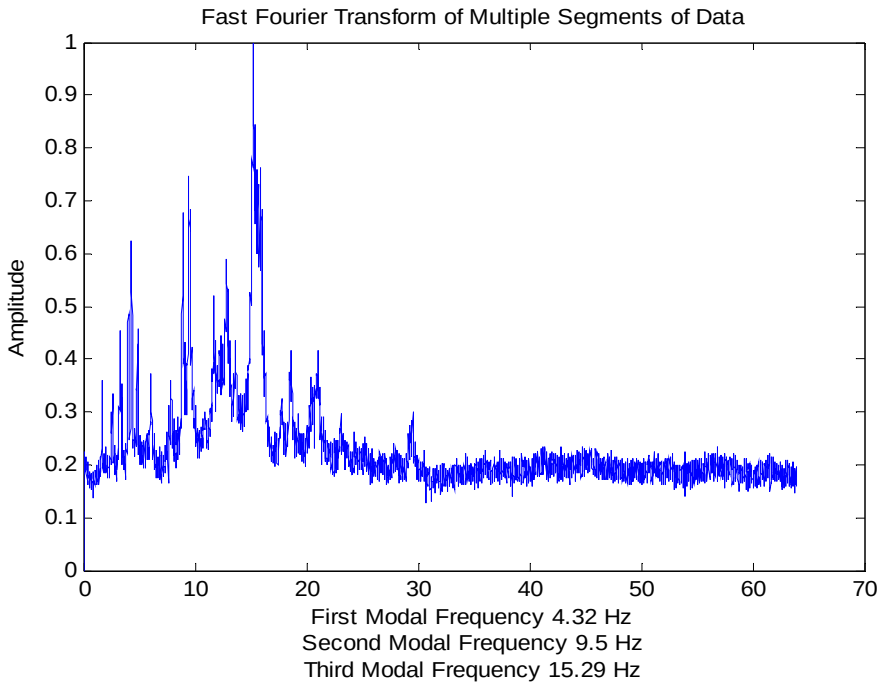

Figure B.8 – FFT of accelerometer data (2:53:07PM, 3/14/2014)